SPECTRAL MEASURE COMPUTATIONS FOR COMPOSITE MATERIALS *

N. B. MURPHY †, E. CHERKAEV ‡, C. HOHENEGGER §, AND K. M. GOLDEN ¶

Abstract. The analytic continuation method of homogenization theory provides Stieltjes integral representations for the effective parameters of composite media, involving spectral measures of self-adjoint random operators which depend only on the composite geometry. On finite bond lattices, these random operators are represented by random matrices and the spectral measures are given explicitly in terms of their eigenvalues and eigenvectors. Here we provide the mathematical foundation for rigorous computation of spectral measures for such composite media. We also introduce a large family of random bond lattices and directly compute the associated spectral measures and effective parameters. The computed spectral measures agree with known theoretical results, and the behavior of the effective parameters is shown to be consistent with rigorous bounds.

Key words. composite materials, random resistor network, percolation, homogenization, spectral measure, random matrix

subject classifications. 00B15, 47B15, 65C60, 30B40, 78A48, 80M40, 60K35

1. Introduction Over the years a broad range of mathematical techniques have been developed that reduce the analysis of complex composite materials, with rapidly varying structures in space, to solving averaged, or *homogenized* equations that do not have rapidly varying data, and involve an effective parameter. Homogenization for the effective parameter problem in composite media with rapidly varying coefficients of thermal conductivity, or equivalently [40] electrical conductivity and permittivity, and magnetic permeability, was developed by Papanicolaou and Varadhan [48] for the steady state, static case. This work was extended [28, 29] by Golden and Papanicolaou to the quasi-static frequency dependent case with complex parameters. Analysis of the effective dielectric problem for the fully frequency dependent case described by the Helmholtz equation is given in [53].

The effective parameter problem for *two-component* media in the quasi-static limit was developed by Bergman [7], Milton [37], and Golden and Papanicolaou [28], leading to Stieltjes integral representations for the effective parameters of composite media. The Golden-Papanicolaou formulation of this analytic continuation method (ACM) is based on the spectral theorem and resolvent formulas involving random self-adjoint operators. This formulation demonstrated that the measures underlying these integral representations are *spectral measures* associated with these random operators, which depend only on the composite geometry. These measures contain all the information about the mixture geometry, and provide a link between microgeometry and transport. Local geometry is encoded in "geometric" resonances in the measures [34], while global connectivity is encoded by spectral gaps in the measures at the spectral endpoints [41, 34]. A remarkable feature of the method is that once the spectral measures are found for a given composite geometry, by the symmetries in the governing equations [40],

*

†University of Utah, Department of Mathematics, 155 S 1400 E RM 233, Salt Lake City, UT 84112-009, USA, (murphy@math.utah.edu)

‡University of Utah, Department of Mathematics, 155 S 1400 E RM 233, Salt Lake City, UT 84112-009, USA, (elena@math.utah.edu).

§University of Utah, Department of Mathematics, 155 S 1400 E RM 233, Salt Lake City, UT 84112-009, USA, (choheneg@math.utah.edu).

¶University of Utah, Department of Mathematics, 155 S 1400 E RM 233, Salt Lake City, UT 84112-009, USA, (golden@math.utah.edu).

the effective electrical, magnetic, and thermal transport properties are *all* completely determined by these measures.

The integral representations yield rigorous *forward bounds* on the effective parameters of composites, given partial information on the microgeometry [7, 37, 28, 8]. One can also use the integral representations to obtain inverse bounds, where data on the electromagnetic response of a sample, for example, is used to bound its structural parameters, such as the volume fractions of the components [13, 11, 14, 57, 9, 12, 15, 27], and even the separation of the inclusions in matrix particle composites [45]. Furthermore, the spectral measure can be *uniquely* reconstructed [11] from effective permittivity data for an interval of electromagnetic frequency which, in turn, can used to recover microstructural parameters [11, 14, 57, 9, 12, 15, 27] and calculate the effective thermal conductivity, viscoelastic modulus, and other effective properties [11, 12]. For classes of composites which undergo a percolation transition, the integral representations have been used to obtain detailed information regarding the critical behavior of the effective parameters in the scaling regime [25, 41]. Furthermore, the relationship between the effective parameters and the system energy has also led to a physically consistent statistical mechanics model for two-component dielectric media which is also mathematically tractable [42].

Despite the many applications which have stemmed from the ACM, explicit computations of the effective parameters have been obtained for only a handful of composite microstructures. To help overcome this limitation, here we develop a mathematical framework which provides a rigorous way to directly compute the spectral measures and effective parameters for finite lattice composite microstructures. A projection method is introduced which provides a numerically efficient way to accomplish these computations. We also introduce a large class of locally isotropic, statistically isotropic, and anisotropic random bond networks and directly compute the associated spectral measures and effective parameters. Our numerical calculations of the spectral measures are in excellent agreement with known theoretical results. Moreover, the behavior of the associated effective parameters are consistent with rigorous bounds.

2. Mathematical Methods We now formulate the effective parameter problem for random two-phase conductive media in the lattice and continuum settings. In Section 2.1 we review and extend the ACM for the continuum setting [28], while the *infinite* lattice setting [10, 23] is reviewed in Section 2.2.1. The mathematical framework underlying the infinite lattice case is analogous to that of the continuum case [10], and the integral representations for the effective parameters follow with minor modifications in the theory. In the *finite* lattice setting, the integral representations for the effective parameters are analogous to that of the continuum and infinite lattice cases. However, significant modifications must be made to the underlying mathematical framework. A key theoretical contribution of this manuscript is the formulation of the ACM for the finite lattice case, which is discussed in Section 2.2.2.

2.1. Continuum Setting Consider a random two-phase conductive medium filling all of $\mathbb{R}^d$, which is determined by the probability space (Ω, P). Here, Ω is the set of all geometric realizations of our random medium, which is indexed by the parameter $\omega \in \Omega$ representing one particular geometric realization, and P is the associated probability measure. Let $\boldsymbol{\sigma}(\vec{x},\omega)$ be the local complex conductivity tensor associated with the conductive medium, which has components $\sigma_{jk}(\vec{x},\omega)$, $j,k=1,\ldots,d$, that are (spatially) stationary random fields.

A *stationary* random field $f \in L^2(\Omega,P)$, $f:\mathbb{R}^d \times \Omega \to \mathbb{R}$, is a field such that the

joint distribution of $f(\vec{x}_1,\omega),\ldots,f(\vec{x}_n,\omega)$ and that of $f(\vec{x}_1+\vec{\xi},\omega),\ldots,f(\vec{x}_n+\vec{\xi},\omega)$ is the same for all $\vec{\xi}\in\mathbb{R}^d$ and $n\in\mathbb{N}$ [28, 48]. In particular, the ensemble average $\langle\cdot\rangle$ of $f(\vec{x},\omega)$ over Ω is invariant under the translation group $\tau_y:\Omega\to\Omega$ defined by $f(\tau_{-y}\vec{x},\omega)=f(\vec{x}+\vec{y},\omega)$ for all $\vec{x},\vec{y}\in\mathbb{R}^d$, with $\tau_x\tau_y=\tau_{x+y}$. Consequently, $\langle f(\vec{x},\omega)\rangle=\langle f(0,\omega)\rangle$ and we can focus on the origin and drop the $\vec{x}$ notation by writing $f(0,\omega)=f(\omega)$, with $f(\tau_{-x}\omega)=f(\vec{x},\omega)$. We shall assume that there is such a group of transformations that is one-to-one and preserves the measure P, i.e. $P(\tau_x A)=P(A)$ for all P-measurable sets A [28, 48].

The group of transformations τ_x acting on Ω induces a group of operators T_x on the Hilbert space $L^2(\Omega,P)$ defined by $(T_x f)(\omega)=f(\tau_{-x}\omega)$ for all $f\in L^2(\Omega,P)$. Since τ_x is measure preserving, the operators T_x form a unitary group and therefore have closed densely defined infinitesimal generators L_i in each direction $i=1,\ldots,d$ with domain $\mathscr{D}_i\subset L^2(\Omega,P)$ [23, 48]. Thus,

$$L_i=\frac{\partial}{\partial x_i}T_x\bigg|_{x=0},\quad i=1,\ldots,d,$$

where x_i is the i^{th} component of the vector $\vec{x}$ and differentiation is defined in the sense of convergence in $L^2(\Omega,P)$ for elements of $\mathscr{D}_i$ [23]. The closed subset $\mathscr{D}=\cap_{i=1}^d\mathscr{D}_i$ of $L^2(\Omega,P)$ is a Hilbert space [23] with inner product $\langle\cdot,\cdot\rangle_D$ given by $\langle f,g\rangle_D=\langle f,g\rangle_{L^2}+\sum_{i=1}^d\langle L_i f,L_i g\rangle_{L^2}$, where $\langle\cdot,\cdot\rangle_{L^2}$ is the $L^2(\Omega,P)$ inner product.

Consider the Hilbert space $\mathscr{H}=\bigotimes_{i=1}^d L^2(\Omega,P)$ with inner product $\langle\cdot,\cdot\rangle$ defined by $\langle\vec{\xi},\vec{\zeta}\rangle=\langle\vec{\xi}\cdot\vec{\zeta}\rangle$, where $\vec{\xi}\cdot\vec{\zeta}=\vec{\xi}^{\,T}\vec{\zeta}$ denotes the dot-product on $\mathbb{R}^d$ and $\langle\cdot\rangle$ means ensemble average over Ω or, by an ergodic theorem [28], spatial average over all of $\mathbb{R}^d$. Define the Hilbert spaces [28] of "curl free" $\mathscr{H}_\times$ and "divergence free" $\mathscr{H}_\bullet$ random fields

$$\begin{aligned}\mathscr{H}_\times&=\Big\{\vec{Y}\in\mathscr{H}\;\big|\;\vec{\nabla}\times\vec{Y}=0\text{ weakly and }\langle\vec{Y}\rangle=0\Big\},\\ \mathscr{H}_\bullet&=\Big\{\vec{Y}\in\mathscr{H}\;\big|\;\vec{\nabla}\cdot\vec{Y}=0\text{ weakly and }\langle\vec{Y}\rangle=0\Big\},\end{aligned}\tag{2.1}$$

where we have used the simplified notation $\langle\vec{Y}\rangle=0\Longleftrightarrow\langle Y_i\rangle=0$ for all $i=1,\ldots,d$, $\vec{\nabla}\cdot\vec{Y}=\sum_{i=1}^d L_iY_i$, and $\vec{\nabla}\times\vec{Y}=0$ means $L_iY_j-L_jY_i=0$ for all $i,j=1,\ldots,d$. Consider the following variational problems [28]. Find $\vec{E}_f\in\mathscr{H}_\times$ and $\vec{J}_f\in\mathscr{H}_\bullet$ such that

$$\langle\boldsymbol{\sigma}(\vec{E}_0+\vec{E}_f)\cdot\vec{Y}\rangle=0\quad\forall\;\vec{Y}\in\mathscr{H}_\times\qquad\text{and}\qquad\langle\boldsymbol{\rho}(\vec{J}_0+\vec{J}_f)\cdot\vec{Y}\rangle=0\quad\forall\;\vec{Y}\in\mathscr{H}_\bullet,\tag{2.2}$$

respectively. When the bilinear forms $\Psi(\vec{\xi},\vec{\zeta})=\boldsymbol{\sigma}\vec{\xi}\cdot\vec{\zeta}$ and $\Phi(\vec{\xi},\vec{\zeta})=\boldsymbol{\rho}\vec{\xi}\cdot\vec{\zeta}$ are bounded and coercive, these problems have unique solutions [28, 48] satisfying the quasi-static limit of Maxwell's equations [33]

$$\begin{aligned}&\vec{\nabla}\times\vec{E}=0,\quad\vec{\nabla}\cdot\vec{J}=0,\quad\vec{J}=\boldsymbol{\sigma}\vec{E},\quad\langle\vec{E}\rangle=\vec{E}_0,\\ &\vec{\nabla}\times\vec{E}=0,\quad\vec{\nabla}\cdot\vec{J}=0,\quad\vec{E}=\boldsymbol{\rho}\vec{J},\quad\langle\vec{J}\rangle=\vec{J}_0.\end{aligned}\tag{2.3}$$

Here, $\vec{E}(\vec{x},\omega)=\vec{E}_0+\vec{E}_f(\vec{x},\omega)$ is the random electric field, where $\vec{E}_0=\langle\vec{E}\rangle$ and $\vec{E}_f$ is the fluctuating field of mean zero about the (constant) average $\vec{E}_0$. Similarly, $\vec{J}(\vec{x},\omega)=\vec{J}_0+\vec{J}_f(\vec{x},\omega)$ is the random current density. Moreover, $\vec{E}_f$ and $\vec{J}_f$ are stationary random fields [28].

As $\vec{E}_f\in\mathscr{H}_\times$ and $\vec{J}_f\in\mathscr{H}_\bullet$, equation (2.2) yields the energy (power) [33] constraints $\langle\vec{J}\cdot\vec{E}_f\rangle=0$ and $\langle\vec{E}\cdot\vec{J}_f\rangle=0$, respectively, which leads to the following reduced energy

representations $\langle \vec{J}\cdot\vec{E}\rangle = \langle \vec{J}\rangle\cdot\vec{E}_0$ and $\langle \vec{E}\cdot\vec{J}\rangle = \langle \vec{E}\rangle\cdot\vec{J}_0$. The effective complex conductivity and resistivity tensors, $\boldsymbol{\sigma}^*$ and $\boldsymbol{\rho}^*$, are defined by

$$\langle \vec{J}\rangle = \boldsymbol{\sigma}^*\vec{E}_0 \quad \text{and} \quad \langle \vec{E}\rangle = \boldsymbol{\rho}^*\vec{J}_0. \tag{2.4}$$

Consequently, $\langle \vec{J}\cdot\vec{E}\rangle = \boldsymbol{\sigma}^*\vec{E}_0\cdot\vec{E}_0 = \boldsymbol{\rho}^*\vec{J}_0\cdot\vec{J}_0$.

We assume that the composite is a locally isotropic medium so that $\sigma_{jk}(\vec{x},\omega) = \sigma(\vec{x},\omega)\delta_{jk}$ and $\rho_{jk}(\vec{x},\omega) = \rho(\vec{x},\omega)\delta_{jk}$, where δ_{jk} is the Kronecker delta and $j,k = 1,\ldots,d$. We further assume that the composite is a two-component medium, so that $\sigma(\vec{x},\omega)$ takes the *complex* values σ_1 and σ_2, and $\rho(\vec{x},\omega)$ takes the values $1/\sigma_1$ and $1/\sigma_2$, and satisfy [28]

$$\sigma(\vec{x},\omega) = \sigma_1\chi_1(\vec{x},\omega) + \sigma_2\chi_2(\vec{x},\omega), \qquad \rho(\vec{x},\omega) = \chi_1(\vec{x},\omega)/\sigma_1 + \chi_2(\vec{x},\omega)/\sigma_2. \tag{2.5}$$

Here, $\chi_i(\vec{x},\omega)$ is the characteristic function of medium $i = 1,2$, which equals one for all $\omega\in\Omega$ having medium i at $\vec{x}$ and zero otherwise, with $\chi_1 = 1-\chi_2$. For simplicity, we focus on one component of these tensors, σ^*_{jk} and ρ^*_{jk}, for some $j,k = 1,\ldots,d$.

Due to the homogeneity of these functions, e.g. $\sigma^*_{jk}(a\sigma_1,a\sigma_2) = a\sigma^*_{jk}(\sigma_1,\sigma_2)$ for any complex number a, they depend only on the ratio $h = \sigma_1/\sigma_2$, and we define the tensor-valued functions $\mathbf{m}(h) = \boldsymbol{\sigma}^*/\sigma_2$, $\mathbf{w}(z) = \boldsymbol{\sigma}^*/\sigma_1$, $\tilde{\mathbf{m}}(h) = \sigma_1\boldsymbol{\rho}^*$, and $\tilde{\mathbf{w}}(z) = \sigma_2\boldsymbol{\rho}^*$ with components

$$m_{jk}(h) = \sigma^*_{jk}/\sigma_2, \quad w_{jk}(z) = \sigma^*_{jk}/\sigma_1, \quad \tilde{m}_{jk}(h) = \sigma_1\rho^*_{jk}, \quad \tilde{w}_{jk}(z) = \sigma_2\rho^*_{jk}. \tag{2.6}$$

where $z = 1/h$. The dimensionless functions $m_{jk}(h)$ and $\tilde{m}_{jk}(h)$ are analytic off the negative real axis in the h-plane, while $w_{jk}(z)$ and $\tilde{w}_{jk}(z)$ are analytic off the negative real axis in the z-plane [28]. Each take the corresponding upper half plane to the upper half plane and are therefore examples of Herglotz functions [16, 28].

A key step in the ACM is obtaining Stieltjes integral representations for $\boldsymbol{\sigma}^*$ and $\boldsymbol{\rho}^*$. These follow from resolvent representations for the electric field [28] and current density [41]

$$\begin{aligned} &\vec{E} = s(sI-\Gamma\chi_1)^{-1}\vec{E}_0 = t(tI-\Gamma\chi_2)^{-1}\vec{E}_0, \quad s\in\mathbb{C}\backslash[0,1], \\ &\vec{J} = t(tI-\Upsilon\chi_1)^{-1}\vec{J}_0 = s(sI-\Upsilon\chi_2)^{-1}\vec{J}_0, \quad t\in\mathbb{C}\backslash[0,1]. \end{aligned} \tag{2.7}$$

Here, we have defined the complex variables $s = 1/(1-h)$ and $t = 1/(1-z) = 1-s$, I is the identity operator on $\mathbb{R}^d$, the operator $\Gamma = \vec{\nabla}(\Delta^{-1})\vec{\nabla}\cdot$ is based on convolution with the free-space Green's function for the Laplacian $\Delta = \vec{\nabla}\cdot\vec{\nabla} = \nabla^2$, and the operator $\Upsilon = -\vec{\nabla}\times(\boldsymbol{\Delta}^{-1})\vec{\nabla}\times$ involves the vector Laplacian $\boldsymbol{\Delta} = -\vec{\nabla}\times\vec{\nabla}\times + \vec{\nabla}\vec{\nabla}\cdot$ [28, 41].

When the current density $\vec{J}(\vec{x},\omega)$ and the electric field $\vec{E}(\vec{x},\omega)$ are sufficiently smooth in a neighborhood of $\vec{x}\in\mathbb{R}^d$ for $\omega\in\Omega$, equation (2.7) is obtained as follows. On the Hilbert space $L^2(\Omega,P)$, the operator Δ^{-1} is well defined in terms of convolution with respect to the free-space Green's function of the Laplacian Δ [28, 20]. Similarly, on the Hilbert space $\mathscr{H} = \bigotimes_{i=1}^d L^2(\Omega,P)$, the inverse $\boldsymbol{\Delta}^{-1}$ of the vector Laplacian $\boldsymbol{\Delta}$ is defined in terms of component-wise convolution with respect to the free-space Green's function of the Laplacian.

Applying the integro-differential operator $\vec{\nabla}(\Delta^{-1})$ to the formula $\vec{\nabla}\cdot\vec{J} = 0$ in equation (2.3) yields $\Gamma\vec{J} = 0$, where $\Gamma = \vec{\nabla}(\Delta^{-1})\vec{\nabla}\cdot$ is an orthogonal projection [28] from $\mathscr{H}$ onto the Hilbert space $\mathscr{H}_\times$ of curl-free random fields, $\Gamma:\mathscr{H}\mapsto\mathscr{H}_\times$. More specifically, for every sufficiently smooth $\vec{\zeta}\in\mathscr{H}_\times$ there exists [33] a scalar potential φ which is unique up to a constant such that $\vec{\zeta} = \vec{\nabla}\varphi$, so that $\Gamma\vec{\zeta} = \vec{\zeta}$.

Similarly we have $\Upsilon\vec{E}=0$, where $\Upsilon=\vec{\nabla}\times(\boldsymbol{\Delta}^{-1})\vec{\nabla}\times$ is an orthogonal projection from $\mathscr{H}$ onto the Hilbert space $\mathscr{H}_\bullet$ of divergence-free random fields (of transverse gauge) [41]. This can be seen as follows. For every sufficiently smooth $\vec{\zeta}\in\mathscr{H}_\bullet$ we have $\vec{\zeta}=\vec{\nabla}\times(\vec{A}+\vec{C})$, where $\vec{A}$ is a vector potential associated with $\vec{\zeta}$ and the arbitrary vector field $\vec{C}$ satisfies $\vec{\nabla}\times\vec{C}=0$ [33]. Without loss of generality, $\vec{C}$ can be chosen so that $\vec{A}$ satisfies $\vec{\nabla}\cdot\vec{A}=0$ [33]. Hence, $\vec{\nabla}\times\vec{\zeta}=\vec{\nabla}\times\vec{\nabla}\times\vec{A}=\vec{\nabla}(\vec{\nabla}\cdot\vec{A})-\boldsymbol{\Delta}\vec{A}=-\boldsymbol{\Delta}\vec{A}$. The vector $\vec{C}$ chosen in this manner gives the transverse *gauge* of $\vec{\zeta}$ [33]. Choosing the members of $\mathscr{H}_\bullet$ to have transverse gauge, the action of $\vec{\nabla}\times\vec{\nabla}\times$ on $\mathscr{H}_\bullet$ is given by that of $-\boldsymbol{\Delta}$. Therefore, the action of Υ on $\mathscr{H}_\bullet$ is given by that of

$$\Upsilon=\vec{\nabla}\times(\vec{\nabla}\times\vec{\nabla}\times)^{-1}\vec{\nabla}\times=\vec{\nabla}\times(\boldsymbol{\Delta}^{-1})\vec{\nabla}\times, \tag{2.8}$$

and it is clear from the above discussion that $\Upsilon\vec{\zeta}=\vec{\zeta}$ for all such $\vec{\zeta}\in\mathscr{H}_\bullet$.

We now derive the formulas in equation (2.7). Write σ and ρ in equation (2.5) as $\sigma=\sigma_2(1-\chi_1/s)=\sigma_1(1-\chi_2/t)$ and $\rho=(1-\chi_2/s)/\sigma_1=(1-\chi_1/t)/\sigma_2$. Note that $\vec{E}=\vec{E}_0+\vec{E}_f$, where $\vec{E}_0$ is a *constant* field and $\vec{E}_f\in\mathscr{H}_\times$ so that $\Gamma\vec{E}=\vec{E}_f$, and similarly $\Upsilon\vec{J}=\vec{J}_f$. Consequently, from $\Gamma\vec{J}=0$ and $\Upsilon\vec{E}=0$ we have the following formulas which are equivalent to that in (2.7)

$$\vec{E}_f=\frac{1}{s}\Gamma\chi_1\vec{E}=\frac{1}{t}\Gamma\chi_2\vec{E},\qquad \vec{J}_f=\frac{1}{t}\Upsilon\chi_1\vec{J}=\frac{1}{s}\Upsilon\chi_2\vec{J}. \tag{2.9}$$

On the Hilbert space $\mathscr{H}_\times$, the operators Γ and χ_i, $i=1,2$, are projectors [28]. Therefore $M_i=\chi_i\Gamma\chi_i$, $i=1,2$, are compositions of projection operators on $\mathscr{H}_\times$, and are consequently positive definite and bounded by 1 in the underlying operator norm [50]. They are self-adjoint with respect to the $\mathscr{H}$-inner-product $\langle\cdot,\cdot\rangle$ [28]. Therefore, on the Hilbert space $\mathscr{H}_\times$ with weight χ_1 in the inner-product, $\langle\cdot,\cdot\rangle_1=\langle\chi_1\cdot,\cdot\rangle$ for example, $\Gamma\chi_1$ is a bounded linear self-adjoint operator with spectrum in the interval $[0,1]$ [28]. Hence the resolvent operator $(sI-\Gamma\chi_1)^{-1}$ in (2.7) is also self-adjoint with respect to the same inner-product, and is bounded for $s\in\mathbb{C}\backslash[0,1]$ [55].

To obtain integral representations for $\boldsymbol{\sigma}^*$ and $\boldsymbol{\rho}^*$, it is more convenient to consider the functions $F_{jk}(s)=\delta_{jk}-m_{jk}(h)$ and $E_{jk}(s)=\delta_{jk}-\tilde{m}_{jk}(h)$ which are analytic off $[0,1]$ in the s-plane, and $G_{jk}(t)=\delta_{jk}-w_{jk}(z)$ and $H_{jk}(t)=\delta_{jk}-\tilde{w}_{jk}(z)$ which are analytic off $[0,1]$ in the t-plane [28]. For the formulation of the effective parameter problem involving $\mathscr{H}_\times$ and $\boldsymbol{\sigma}^*$, define the coordinate system so that in (2.4) the constant vector $\vec{E}_0$ is given by $\vec{E}_0=E_0\vec{e}_j$, where $\vec{e}_j$ is the standard basis vector on $\mathbb{R}^d$ in the j^{th} direction for some $j=1,\ldots,d$. In the other formulation involving $\mathscr{H}_\bullet$ and $\boldsymbol{\rho}^*$, define $\vec{J}_0=J_0\vec{e}_j$. Equations (2.4) and (2.7), and the spectral theorem for bounded linear self-adjoint operators [49, 55] then yield the following integral representations [28, 6, 8, 41] for the effective parameters σ^*_{jk} and ρ^*_{jk} (see Section A-1.1.1 for details)

$$\begin{aligned}
&m_{jk}(h)=\delta_{jk}-F_{jk}(s),\qquad F_{jk}(s)=\langle\chi_1(sI-\Gamma\chi_1)^{-1}\vec{e}_j\cdot\vec{e}_k\rangle=\int_0^1\frac{\mu_{jk}(d\lambda)}{s-\lambda},\\
&w_{jk}(z)=\delta_{jk}-G_{jk}(t),\qquad G_{jk}(t)=\langle\chi_2(tI-\Gamma\chi_2)^{-1}\vec{e}_j\cdot\vec{e}_k\rangle=\int_0^1\frac{\alpha_{jk}(d\lambda)}{t-\lambda},\\
&\tilde{m}_{jk}(h)=\delta_{jk}-E_{jk}(s),\qquad E_{jk}(s)=\langle\chi_2(sI-\Upsilon\chi_2)^{-1}\vec{e}_j\cdot\vec{e}_k\rangle=\int_0^1\frac{\eta_{jk}(d\lambda)}{s-\lambda},\\
&\tilde{w}_{jk}(z)=\delta_{jk}-H_{jk}(t),\qquad H_{jk}(t)=\langle\chi_1(tI-\Upsilon\chi_1)^{-1}\vec{e}_j\cdot\vec{e}_k\rangle=\int_0^1\frac{\kappa_{jk}(d\lambda)}{t-\lambda}.
\end{aligned} \tag{2.10}$$

Here, μ_{jk} and α_{jk} are *spectral measures* associated with the random operators $\chi_1\Gamma\chi_1$ and $\chi_2\Gamma\chi_2$, respectively, while η_{jk} and κ_{jk} are spectral measures associated with the random operators $\chi_2\Upsilon\chi_2$ and $\chi_1\Upsilon\chi_1$, respectively. More specifically, for example, $\mu_{jk}(d\lambda) = \langle R(d\lambda)\vec{e}_j, \vec{e}_k\rangle_1$, where $R(d\lambda)$ is the projection valued measure associated with the operator $\chi_1\Gamma\chi_1$ acting on $\mathscr{H}_\times$ (see Section A-1.1 for more details).

By the Stieltjes–Perron inversion theorem [32, 40] the spectral measure $\boldsymbol{\mu}$, for example, is given by the weak limit $\boldsymbol{\mu}(d\lambda) = -\lim_{\epsilon\downarrow 0}\mathrm{Im}(\mathbf{F}(\lambda+\mathrm{i}\epsilon))(d\lambda/\pi)$, i.e.

$$\int_0^1 \xi(\lambda)\,\boldsymbol{\mu}(d\lambda) = -\frac{1}{\pi}\lim_{\epsilon\downarrow 0}\int_0^1 \xi(\lambda)\,\mathrm{Im}(\mathbf{F}(\lambda+\mathrm{i}\epsilon))\,d\lambda, \tag{2.11}$$

for all smooth scalar test functions $\xi(\lambda)$, where $(\mathbf{F}(s))_{jk} = F_{jk}(s)$. From equation (2.11) and the identities $m_{jk}(h) = h\,w_{jk}(z)$ and $\tilde{m}_{jk}(h) = h\,\tilde{w}_{jk}(z)$, which follow from equation (2.6), it can be shown [41] that the measures μ_{jk} and α_{jk}, and the measures η_{jk} and κ_{jk} are related by

$$\begin{aligned}
\lambda\alpha_{jk}(\lambda) &= (1-\lambda)\mu_{jk}(1-\lambda) + \lambda(\,m_{jk}(0)\delta_0(d\lambda) + w_{jk}(0)(\lambda-1)\delta_1(d\lambda)\,),\\
\lambda\kappa_{jk}(\lambda) &= (1-\lambda)\eta_{jk}(1-\lambda) + \lambda(\,\tilde{m}_{jk}(0)\delta_0(d\lambda) + \tilde{w}_{jk}(0)(\lambda-1)\delta_1(d\lambda)\,).
\end{aligned} \tag{2.12}$$

Here, $m(0) = m(h)|_{h=0}$ and $w(0) = w(z)|_{z=0}$, for example, and $\delta_a(d\lambda)$ is the delta measure concentrated at $\lambda = a$. Equations (2.10) and (2.12) demonstrate the many symmetries between the functions $m_{jk}(h)$, $w_{jk}(z)$, $\tilde{m}_{jk}(h)$, and $\tilde{w}_{jk}(z)$, and the respective measures μ_{jk}, α_{jk}, η_{ij}, and κ_{jk}. Because of these symmetries, for simplicity, we will focus on $m_{jk}(h)$ and μ_{jk}, and will reintroduce the other functions and measures where appropriate.

A key feature of equations (2.4), (2.6), and (2.10) is that the parameter information in h and E_0 is *separated* from the geometry of the composite, which is encoded in the spectral measure μ_{jk} via its moments $\mu_{jk}^n = \int_0^1 \lambda^n \mu_{jk}(d\lambda)$, $n = 0,1,2,\ldots$. For example, the mass μ_{jk}^0 of the measure μ_{jk} is given by $\mu_{jk}^0 = p_1\delta_{jk}$, where $p_1 = \langle\chi_1\rangle$ is the volume fraction of material component 1. To see this, recall from Section A-1.1.1 that the projection valued measure $R(d\lambda)$ satisfies $\int_0^1 R(d\lambda) = I$. Moreover, recall that the associated operator $R(\lambda)$ is a *self-adjoint projector* on $\mathscr{H}_\times$ for $\lambda\in[0,1]$ [49, 55]. Consequently, we have

$$\begin{aligned}
\mu_{jk}^0 &= \int_0^1 \mu_{jk}(d\lambda) = \int_0^1 \langle R(d\lambda)\vec{e}_j\cdot\vec{e}_k\rangle_1 = \langle 1\rangle_1\,\vec{e}_j\cdot\vec{e}_k = \langle\chi_1\rangle\,\delta_{jk},\\
\mu_{kk}(d\lambda) &= \langle R(d\lambda)\vec{e}_k\cdot\vec{e}_k\rangle_1 = \langle R(d\lambda)\vec{e}_k\cdot R(d\lambda)\vec{e}_k\rangle_1 = \|R(d\lambda)\vec{e}_k\|_1^2,
\end{aligned} \tag{2.13}$$

where we have used a Fubini theorem [21] and $\|\cdot\|_1$ denotes the norm induced by the inner-product $\langle\cdot,\cdot\rangle_1$. From equation (2.13) we see, generically, that the diagonal components μ_{kk}, $k=1,\ldots,d$, of $\boldsymbol{\mu}$ are positive measures of mass p_1, while the off-diagonal components μ_{jk}, $j\neq k = 1,\ldots,d$, have zero mass and are consequently signed measures [21, 50].

The higher order moments μ_{jk}^n, $n=1,2,3,\ldots$, in principle, may be found using a perturbation expansion of $F_{jk}(s)$ about a homogeneous medium ($\sigma_1=\sigma_2$, $s=\infty$) [28]. In particular $\mu_{jk}^0 = p_1\delta_{jk}$, generically, and $\mu_{jk}^1 = (p_1p_2/d)\,\delta_{jk}$ for a statistically isotropic random medium [28, 26, 10], where $p_2 = 1-p_1 = \langle\chi_2\rangle$ is the volume fraction of material component 2. In the case of a square bond lattice, which is an example of an infinitely interchangeable random medium, $\mu_{kk}^2 = p_1p_2(1+(d-2)p_2)/d^2$ for any dimension d and $\mu_{kk}^3 = p_1p_2(p_2^2-p_2-1)/8$ for $d=2$. In general, the moments μ_{jk}^n depend on the $(n+1)$-point correlation functions of the random medium [28, 10].

A principal application of the ACM is to derive *forward bounds* on the diagonal components σ^*_{kk} of the tensor $\boldsymbol{\sigma}^*$, $k=1,\ldots,d$, given partial information on the microgeometry [7, 37, 28, 8]. This information may be given in terms of the moments μ^n_{kk}, $n=0,1,2,\ldots$, of the measure μ_{kk} [39, 28]. Given this information, the bounds on σ^*_{kk} follow from the special structure of $F_{kk}(s)$ in (2.10). More specifically, it is a *linear* functional of the *positive* measure μ_{kk}. The bounds are obtained by fixing the contrast parameter s, varying over an admissible set of measures μ_{kk} (or geometries) which is determined by the known information regarding the two-component composite. Knowledge of the moments μ^n_{kk} for $n=1,\ldots,J$ confines σ^*_{kk} to a region of the complex plane which is bounded by arcs of circles, and the region becomes progressively smaller as more moments are known [39, 22]. When all the moments are known the measure μ_{kk} is uniquely determined [1], hence σ^*_{kk} is explicitly known. The bounding procedure is reviewed in Section 2.3.

We conclude this section with some final remarks regarding the energy constraints $\langle\vec{J}\cdot\vec{E}_f\rangle=0=\langle\vec{E}\cdot\vec{J}_f\rangle$, which follow from equation (2.2) and are at the heart of the existence and uniqueness of solutions to equation (2.3). We first note that the formulas $\Gamma\vec{E}=\vec{E}_f$ and $\Upsilon\vec{J}=\vec{J}_f$ are sufficient conditions for these constraints. The sufficiency of these conditions can be seen by writing $\sigma=\sigma_2(1-\chi_1/s)$ and $\rho=(1-\chi_1/t)/\sigma_2$ in $\vec{J}=\sigma\vec{E}$ and $\vec{E}=\rho\vec{J}$, respectively, to obtain

$$\langle\vec{J}\cdot\vec{E}_f\rangle=\sigma_2(\langle\vec{E}\cdot\vec{E}_f\rangle-\langle\chi_1\vec{E}\cdot\vec{E}_f\rangle/s),\quad \langle\vec{E}\cdot\vec{J}_f\rangle=(\langle\vec{J}\cdot\vec{J}_f\rangle-\langle\chi_1\vec{J}\cdot\vec{J}_f\rangle/t)/\sigma_2,\quad (2.14)$$

for $s\neq 0$ ($h\neq\pm\infty$) and $t\neq 0$ ($h\neq 0$). Now, if we have $\Gamma\vec{E}=\vec{E}_f$ then $\vec{\nabla}\cdot\vec{J}=0$ yields equation (2.9) ($\vec{E}_f=\Gamma\chi_1\vec{E}/s$). Therefore, as Γ is a self-adjoint operator on $\mathscr{H}$ [20], we have

$$\langle\chi_1\vec{E}\cdot\vec{E}_f\rangle=\langle\chi_1\vec{E}\cdot\Gamma\vec{E}\rangle=\langle\Gamma\chi_1\vec{E}\cdot\vec{E}\rangle=s\langle\vec{E}_f\cdot\vec{E}\rangle.\quad (2.15)$$

Consequently, from equation (2.14) we have $\langle\vec{J}\cdot\vec{E}_f\rangle=0$ for $s\neq 0$. The argument involving the operator Υ and the vector field $\vec{J}_f$ is analogous.

We see from equation (2.14) that the energy constraints are equivalent to the following "field representations" for the contrast parameters s and t

$$\langle\chi_1\vec{E}\cdot\vec{E}_f\rangle/\langle\vec{E}\cdot\vec{E}_f\rangle=s=1-t=1-\langle\chi_1\vec{J}\cdot\vec{J}_f\rangle/\langle\vec{J}\cdot\vec{J}_f\rangle,\quad (2.16)$$

when $\langle\vec{E}\cdot\vec{E}_f\rangle\neq 0$ (if and only if $\langle\chi_1\vec{E}\cdot\vec{E}_f\rangle\neq 0$), for example. We also note that equation (2.16) provides a relationship between the members $\vec{E}_f$ and $\vec{J}_f$ of the Hilbert spaces $\mathscr{H}_\times$ and $\mathscr{H}_\bullet$, respectively. Moreover, since $h=1-1/s$ and $h\geq 0$ for $h\in\mathbb{R}$, this implies, for example, that $|\langle\vec{E}\cdot\vec{E}_f\rangle|\leq|\langle\chi_1\vec{E}\cdot\vec{E}_f\rangle|$ for $h\in\mathbb{R}$. Furthermore, the energy constraints provide the limiting behavior of the ratio $\mathcal{R}(h)=\langle\vec{E}\cdot\vec{E}_f\rangle/\langle\chi_1\vec{E}\cdot\vec{E}_f\rangle=1/s$

$$\lim_{h\to 0}\mathcal{R}(h)=1,\quad \lim_{h\to 1}\mathcal{R}(h)=0,\quad \lim_{h\to+\infty}\mathcal{R}(h)=-\infty,$$

which is otherwise a very complicated object in the absence of these energy constraints.

The energy constraints also lead to detailed decompositions of the system energy $\langle\vec{J}\cdot\vec{E}\rangle$ in terms of Herglotz functions involving the measures μ_{jj}, α_{jj}, η_{jj}, and κ_{jj} [41, 42]. For example, $\langle\vec{J}\cdot\vec{E}_f\rangle=0$, $\vec{E}=\vec{E}_0+\vec{E}_f$, $\vec{E}_0=E_0\vec{e}_j$, $\langle\vec{E}_f\rangle=0$, and $\sigma=\sigma_2(1-\chi_1/s)$ together imply that $0=\langle\sigma\vec{E}\cdot\vec{E}_f\rangle=\langle\sigma_2(1-\chi_1/s)(\vec{E}_f\cdot\vec{E}_0+E_f^2)\rangle=$

$\sigma_2\left[\langle E_f^2\rangle - (\langle\chi_1\vec{E}_f\cdot\vec{E}_0\rangle + \langle\chi_1 E_f^2\rangle)/s\right]$. Equations (2.7) and (2.10), and the spectral theorem [49] then yield [41, 42]

$$\frac{\langle E_f^2\rangle}{E_0^2} = \int_0^1 \frac{\lambda\mu_{jj}(d\lambda)}{(s-\lambda)^2} = \int_0^1 \frac{\lambda\alpha_{jj}(d\lambda)}{(t-\lambda)^2}. \tag{2.17}$$

Equation (2.17), in turn, leads to Herglotz representations of all such energy components involving these measures [42]. Analogous energy decompositions involving $\vec{J}_f$ and the measures η_{jj} and κ_{jj} similarly follow. In [42] this energy decomposition has lead to a physically transparent statistical mechanics model of two-phase dielectric media.

2.2. Lattice Setting In this section we formulate the effective parameter problem for the infinite and finite, two-component bond lattice on $\mathbb{Z}^d$. The infinite bond lattice, reviewed in Section 2.2.1, is a special case of the stationary random medium considered in Section 2.1. In Section 2.2.2 we develop the mathematical framework for the ACM in the finite lattice setting, a key theoretical contribution of this work.

2.2.1. Infinite Lattice Setting Consider a two-component bond lattice on all of $\mathbb{Z}^d$ determined by the probability space (Ω,P), and let $\boldsymbol{\sigma}(\vec{x},\omega)$ be the local complex conductivity tensor with components $\sigma_{jk}(\vec{x},\omega)=\sigma^j(\vec{x},\omega)\delta_{jk}$, $j,k=1,\ldots,d$. Here $\sigma^j(\vec{x},\omega)$ is the conductivity of the bond emanating from $\vec{x}\in\mathbb{Z}^d$ in the positive j^{th} direction, which is a stationary random field that takes the *complex* values σ_1 and σ_2 with probabilities p_1 and $p_2=1-p_1$, respectively [23, 10]. The configuration space $\Omega=\{\sigma_1,\sigma_2\}^{d\mathbb{Z}^d}$ represents the set of all realizations of the random medium and the probability measure P is compatible with stationarity. Analogous to equation (2.5), the local conductivity $\sigma^j(\vec{x},\omega)$ of the two-phase random medium takes the form [23]

$$\sigma^j(\vec{x},\omega)=\sigma_1\chi_1^j(\vec{x},\omega)+\sigma_2\chi_2^j(\vec{x},\omega),\quad j=1,\ldots,d. \tag{2.18}$$

Here, $\chi_i^j(\vec{x},\omega)$ is the characteristic function of medium $i=1,2$, which equals one for all realizations $\omega\in\Omega$ having medium i in the j^{th} positive bond at $\vec{x}$, and equals zero otherwise.

In this lattice setting, the differential operators $\vec{\nabla}\times$ and $\vec{\nabla}\cdot$ in equation (2.3) are given [23, 10] in terms of forward and backward difference operators D_j^+ and D_j^-, respectively, where

$$D_j^+=T_j^+-I,\quad D_j^-=I-T_j^-,\quad j=1,\ldots,d. \tag{2.19}$$

Here, I is the identity operator on $\mathbb{Z}^d$, and $T_j^+=T_{+e_j}$ and $T_j^-=T_{-e_j}$ are the generators (through composition) of the unitary group T_x acting on $L^2(\Omega,P)$ defined by $(T_xf)(0,\omega)=f(\vec{x},\omega)$, for any $f\in L^2(\Omega,P)$ which is a stationary random field [23]. Define $\mathscr{H}=\bigotimes_{i=1}^d L^2(\Omega,P)$ and let $\vec{E},\vec{J}\in\mathscr{H}$ be the random electric field and current density, respectively, where $\vec{E}(\vec{x},\omega)=(E^1(\vec{x},\omega),\ldots E^d(\vec{x},\omega))$ and $E^j(\vec{x},\omega)$ is the electric field in the bond emanating from $\vec{x}$ in the positive j^{th} direction, and similarly for $\vec{J}(\vec{x},\omega)$.

As in Section 2.1 we write $\vec{E}=\vec{E}_0+\vec{E}_f$, where $\vec{E}_f$ is the fluctuating field of mean zero about the (constant) average $\vec{E}_0$. The variational problem in (2.2) for this lattice

setting has a unique solution satisfying Kirchhoff's circuit laws [28, 10]

$$D_i^+ E^j - D_j^+ E^i = 0, \quad \sum_{k=1}^{d} D_k^- J^k = 0, \quad J^i = \sigma^i E^i, \quad \langle \vec{E} \rangle = \vec{E}_0, \tag{2.20}$$

where $i,j=1,\ldots,d$ and the components $E^i(\vec{x},\omega)$ and $J^i(\vec{x},\omega)$ of $\vec{E}(\vec{x},\omega)$ and $\vec{J}(\vec{x},\omega)$ are stationary random fields. Equation (2.20) is a direct analogue of equation (2.3) when written in component form [28]. Analogous to equation (2.4), the effective complex conductivity tensor $\boldsymbol{\sigma}^*$ is defined by $\langle \vec{J} \rangle = \boldsymbol{\sigma}^* \vec{E}_0$, and has components $\sigma^*_{jk} = \sigma_2 m_{jk}(h)$, $j,k=1,\ldots,d$, where $h=\sigma_1/\sigma_2$. The representation formula for $m_{jk}(h)$ in (2.10) still holds in this infinite lattice setting, with Γ in (2.7) now given by

$$\Gamma = \nabla^+ (\Delta^{-1}) \nabla^-, \quad \nabla^\pm = (D_1^\pm, \ldots, D_d^\pm), \tag{2.21}$$

where Δ^{-1} is based on discrete convolution with the lattice Green's function for the Laplacian $\Delta = \nabla^2$ [10]. The formulation of the ACM for the effective resistivity tensor $\boldsymbol{\rho}^*$ in the infinite lattice setting is analogous to that for $\boldsymbol{\sigma}^*$ given here.

2.2.2. Finite Lattice Setting Consider a finite, two-component bond lattice on $\mathbb{Z}_L^d \subset \mathbb{Z}^d$ determined by the probability space (Ω, P), where

$$\mathbb{Z}_L^d = \{\vec{x} \in \mathbb{Z}^d \mid 1 \le x_i \le L,\ i=1,\ldots,d\}, \tag{2.22}$$

$L \in \mathbb{N}$, $L \ge 2$, and $x_i = (\vec{x})_i$ is the i^{th} component of the vector $\vec{x}$. Let $\boldsymbol{\sigma}(\vec{x},\omega)$ be the local complex conductivity tensor with components $\sigma_{jk}(\vec{x},\omega) = \sigma^j(\vec{x},\omega)\delta_{jk},\ j,k=1,\ldots,d$, where $\sigma^j(\vec{x},\omega)$ is defined in equation (2.18) for $\vec{x} \in \mathbb{Z}_L^d$ and $\omega \in \Omega$. The configuration space $\Omega = \{\sigma_1, \sigma_2\}^{d\mathbb{Z}_L^d}$ represents the set of all 2^N realizations of the finite random bond lattice, where $N = dL^d$, and P is the associated probability measure. Define $\mathscr{H} = \bigotimes_{i=1}^d L^2(\Omega, P)$ and let $\vec{E}, \vec{J} \in \mathscr{H}$ be the random electric field and current density, respectively, which satisfy Kirchhoff's circuit laws (2.20) with appropriate boundary conditions. Analogous to equation (2.4), the effective complex conductivity tensor $\boldsymbol{\sigma}^*$ is defined by $\langle \vec{J} \rangle = \boldsymbol{\sigma}^* \vec{E}_0$, and has components $\sigma^*_{jk} = \sigma_2 m_{jk}(h)$, $\vec{E}_0 = \langle \vec{E} \rangle$, and $\langle \cdot \rangle$ denotes ensemble average over Ω.

In this section we obtain discrete versions of the integral representations for $m_{jk}(h)$ and $\tilde{w}_{jk}(z)$ in (2.10) for this finite bond lattice setting, involving spectral measures μ_{jk} and κ_{jk} associated with real-symmetric random matrices. The integral representations for $\tilde{m}_{jk}(h)$ and $w_{jk}(z)$ are analogous. Toward this goal, we define a bijective mapping Θ from the two-dimensional set $\mathbb{Z}_L^d$ onto the one dimensional set $\mathbb{N}_L \subset \mathbb{N}$ given by

$$\mathbb{N}_L = \{i \in \mathbb{N} \mid i \le dL^d\}, \qquad \Theta(\vec{x}) = x_1 + \sum_{k=2}^{d} (x_k - 1) L^{k-1}. \tag{2.23}$$

Under the bijection Θ the components $E^j(\vec{x},\omega)$, $j=1,\ldots,d$, of the random electric field $\vec{E}(\vec{x},\omega) = (E^1(\vec{x},\omega),\ldots,E^d(\vec{x},\omega))$ are mapped to vector valued functions $E^j(\vec{x},\omega) \mapsto \vec{E}^j(\omega) = (E_1^j(\omega),\ldots,E_{L^d}^j(\omega))$ so that

$$\Theta(\vec{E}(\vec{x},\omega)) = (\vec{E}^1(\omega),\ldots,\vec{E}^d(\omega)) \in \mathbb{R}^N \tag{2.24}$$

for each $\omega \in \Omega$, and similarly for $\vec{J}(\vec{x},\omega)$. Moreover, the bijection Θ maps the standard basis vector $\vec{e}_1 = (1,0,\ldots,0) \in \mathbb{Z}^d$, for example, to the vector $(\vec{1},\vec{0},\ldots,\vec{0}) \in \mathbb{Z}^N$, where $\vec{1}$

and $\vec{0}$ are vectors of ones and zeros of length L^d, respectively, and similarly for the $\vec{e}_j$ for $j=2,\ldots,d$. Therefore, the vectors $\hat{e}_i=\Theta(\vec{e}_i)/L^{d/2}$, $i=1,\ldots,d$, serve as the standard basis vectors on $\mathbb{N}_L$, with $\hat{e}_i\cdot\hat{e}_j=\delta_{ij}$.

On $\mathbb{N}_L$ the difference operators $D_j^{\pm}$, $j=1,\ldots,d$, in equation (2.19) are given in terms of finite difference matrices D_j [17]. Moreover, the Laplacian Δ and the projection operator Γ in (2.21) are replaced by the real-symmetric matrices $\Delta=\nabla^T\nabla$ and $\Gamma=\nabla(\Delta^{-1})\nabla^T$, respectively, where $\nabla=(D_1,\ldots,D_d)^T$. The matrices Δ and Γ depend only on the topology and the boundary conditions of the underlying finite bond lattice $\mathbb{Z}_L^d$, and Γ is a projection matrix satisfying $\Gamma^2=\Gamma$.

The projection matrix representation of the operator Υ on $\mathbb{N}_L$ is obtained as follows. In three dimensions the curl operation $\vec{\nabla}\times$ is given by

$$\vec{\nabla}\times\vec{\zeta}=\mathrm{Det}\begin{bmatrix}\vec{e}_1 & \vec{e}_2 & \vec{e}_3\\ \partial_1 & \partial_2 & \partial_3\\ \zeta_1 & \zeta_2 & \zeta_3\end{bmatrix}=C\vec{\zeta},\quad C=\begin{bmatrix}0 & -\partial_3 & \partial_2\\ \partial_3 & 0 & -\partial_1\\ -\partial_2 & \partial_1 & 0\end{bmatrix},\tag{2.25}$$

where $\vec{\zeta}=\vec{\zeta}(\vec{x})$ for $\vec{x}\in\mathbb{R}^3$, we have denoted ∂_i, $i=1,2,3$, to be partial differentiation in the i^{th} direction $\vec{e}_i$, and C is the curl operator $\vec{\nabla}\times$ in matrix form. One can check directly that $C^2=-C^TC=-\boldsymbol{\Delta}+\vec{\nabla}\vec{\nabla}\cdot$, where $\boldsymbol{\Delta}$ is the vector Laplacian. For dimensions $d>3$, the condition $\vec{\nabla}\times\vec{\zeta}=0$ is given by $\partial_j\zeta_j-\partial_j\zeta_i=0$, $i,j=1,\ldots,d$, [28]. Consequently, the matrix curl operator C analogous to that in (2.25) for $d>3$ becomes increasingly rectangular with increasing dimension. The two-dimensional case follows from (2.25) by setting $\vec{\zeta}(\vec{x})=[\zeta_1(\vec{x}),\zeta_2(\vec{x}),0]^T$ with $\vec{x}=[x_1,x_2,0]^T$, yielding

$$\vec{\nabla}\times\vec{\zeta}=(\partial_1\zeta_2-\partial_2\zeta_1)\vec{e}_3=(\vec{\nabla}\cdot R\vec{\zeta}_2)\vec{e}_3,\quad \vec{\nabla}\cdot=\begin{bmatrix}\partial_1 & \partial_2\end{bmatrix},\quad R=\begin{bmatrix}0 & 1\\ -1 & 0\end{bmatrix},\tag{2.26}$$

where R is a 90° rotation matrix, we have defined $\vec{\zeta}_2=[\zeta_1\ \zeta_2]^T$, and the action of $\vec{\nabla}\cdot R$ on $\vec{\zeta}_2$ is given by that of the operator $[-\partial_2\ \partial_1]$.

In view of equation (2.25), the matrix representation of the curl operator $\vec{\nabla}\times$ on $\mathbb{N}_L$ in *three dimensions* is given by C in (2.25) under the mapping $\partial_i\mapsto D_i$, $i=1,2,3$. In two dimensions, pointwise rotations of fields by 90° convert curl free fields to divergence free fields, and vice versa [40]. With this in mind and in view of equation (2.26), in *two dimensions* it is natural to define the curl operator by $\vec{\nabla}\times=\vec{\nabla}\cdot R=[-\partial_2\ \partial_1]$ so that on $\mathbb{N}_L$ we have

$$\vec{\nabla}\times\vec{\zeta}=C^T\vec{\zeta},\quad C^T=\begin{bmatrix}-D_2 & D_1\end{bmatrix},\tag{2.27}$$

where C satisfies $C^TC=\nabla^T\nabla=\Delta$, the matrix representation of the Laplacian. From the above discussion and in view of equation (2.8), it is natural to define the matrix representation of Υ on $\mathbb{N}_L$ by

$$\Upsilon=C(C^TC)^{-1}C^T,\tag{2.28}$$

which is clearly a projection matrix $\Upsilon^2=\Upsilon$.

We now discuss the matrix representation of the characteristic function $\chi_1^j(\vec{x},\omega)$ on $\mathbb{N}_L$. By writing the constitutive relation $J^j(\vec{x},\omega)=\sigma^j(\vec{x},\omega)E^j(\vec{x},\omega)$ displayed in equation (2.20) as $J^j(\vec{x},\omega)=\sigma_2(1-\chi_1^j(\vec{x},\omega)/s)E^j(\vec{x},\omega)$, we see that the characteristic function $\chi_1^j(\vec{x},\omega)$ in (2.18) operates, according to the probability measure P, on the electric field $E^j(\vec{x},\omega)$ in each individual bond $j=1,\ldots,d$ emanating from $\vec{x}\in\mathbb{Z}_L^d$. In

view of this and equation (2.24), on $\mathbb{N}_L$ the characteristic function $\chi_1^j(\vec{x},\omega)$ is represented by a block diagonal matrix

$$\chi_1(\omega) = \text{diag}(\chi_1^1(\omega),\ldots,\chi_1^d(\omega)), \tag{2.29}$$

where $\chi_1^j(\omega)$, $j=1,\ldots,d$, is a diagonal matrix of size $L^d \times L^d$ with zeros and ones distributed according to P along the main diagonal. Moreover, the matrix $\chi_1^j(\omega)$ acts on the vector $\vec{E}^j(\omega) = \Theta(E^j(\vec{x},\omega))$ in (2.24) for each $j=1,\ldots,d$. Consequently, $\chi_1(\omega)$ is also a real-symmetric projection matrix of size $N \times N$, which determines the geometry and component connectivity of the two-phase random medium. In summary, on $\mathbb{N}_L$ the operators $M_1 = \chi_1\Gamma\chi_1$ and $K_1 = \chi_1\Upsilon\chi_1$ are represented by real-symmetric random matrices of size $N \times N$ [27, 41]. The matrix representations of the operators $M_2 = \chi_2\Gamma\chi_2$ and $K_2 = \chi_2\Upsilon\chi_2$ are analogously determined with use of the identity $\chi_2(\omega) = I - \chi_1(\omega)$, where I is the identity matrix on $\mathbb{R}^N$.

We now discuss the fundamental difference in the mathematical framework between the *infinite* settings formulated in Sections 2.1, 2.2.1, and A-1.1.1, and the *finite* lattice setting formulated here and in Section A-1.1.2. In the infinite settings, the (infinite-dimensional) operator $\Gamma\chi_1$ appears in the integral representation (2.10) for the effective parameters, involving the $\mathscr{H}$-inner-product weighted by $\chi_1(\vec{x},\omega)$. In this abstract (infinite-dimensional) Hilbert space formulation of the effective parameter problem, the resolvent $(sI - \Gamma\chi_1)^{-1}$ is a linear self-adjoint operator which is bounded for $s \in \mathbb{C}\backslash[0,1]$ [55]. In contrast, the finite lattice formulation of the effective parameter problem involves a finite dimensional Hilbert space, and the operators Γ and χ_1 are matrices. In this case, the matrix $\Gamma\chi_1$ is *not* symmetric, it typically has complex spectrum, and it may not even have a full set of eigenvectors. Consequently, the integral formulas in equations (A-3) and (A-4), which were derived for the *symmetric* matrix $M_1 = \chi_1\Gamma\chi_1$, fail to hold for the matrix $\Gamma\chi_1$ in general. Due to this fundamental difference in the theory for the finite lattice setting, the mathematical framework must be significantly modified from that for the infinite settings. The ACM for the finite lattice case is summarized by the following theorem, which is given in terms of the random matrix M_1. The formulations for the matrices M_2 and K_i, $i=1,2$, are analogous.

THEOREM 2.1. *For each $\omega \in \Omega$, let $N_1(\omega) = \text{Trace}(\chi_1(\omega))$ be the number of ones along the main diagonal of $\chi_1(\omega)$, with $N_0(\omega) = N - N_1(\omega)$. Also, let $M_1(\omega) = U(\omega)\Lambda(\omega)U(\omega)$ be the spectral decomposition of $M_1(\omega)$. Here, the columns of $U(\omega)$ consist of the orthonormal eigenvectors $\vec{u}_i(\omega)$, $i=1,\ldots,N$, of $M_1(\omega)$ and the diagonal matrix $\Lambda(\omega) = \text{diag}(\lambda_1(\omega),\ldots,\lambda_N(\omega))$ involves its eigenvalues $\lambda_i(\omega)$. Then, there exists a permutation matrix $\Pi(\omega)$ of size $N \times N$, an orthogonal matrix $U_1(\omega)$ of size $N_1(\omega) \times N_1(\omega)$, and a diagonal matrix $\Lambda_1(\omega)$ of size $N_1(\omega) \times N_1(\omega)$ such that*

$$U = \Pi^T \begin{bmatrix} I_0 & 0_{01} \\ 0_{10} & U_1 \end{bmatrix}, \qquad \Lambda = \begin{bmatrix} 0_{00} & 0_{01} \\ 0_{10} & \Lambda_1 \end{bmatrix}, \tag{2.30}$$

where I_0 is the identity matrix of size $N_0(\omega) \times N_0(\omega)$ and 0_{ab} is a matrix of zeros of size $N_a(\omega) \times N_b(\omega)$, for $a,b=0,1$. Moreover, if the electric field $\vec{E}(\omega)$ satisfies $\vec{E}(\omega) = \vec{E}_0 + \vec{E}_f(\omega)$, with $\vec{E}_0 = \langle \vec{E}(\omega) \rangle$ and $\Gamma\vec{E}(\omega) = \vec{E}_f(\omega)$, then the effective complex

conductivity tensor $\boldsymbol{\sigma}^*$ *has components* $\sigma^*_{jk} = \sigma_2 m_{jk}(h)$, $j,k = 1,\ldots,d$, *which satisfy*

$$m_{jk}(h) = \delta_{jk} - F_{jk}(s), \quad F_{jk}(s) = \int_0^1 \frac{\mu_{jk}(d\lambda)}{s-\lambda}, \quad \mu_{jk}(d\lambda) = \sum_{i=1}^{N} \langle \delta_{\lambda_i}(d\lambda) \chi_1 R_i \hat{e}_j \cdot \hat{e}_k \rangle. \tag{2.31}$$

where $R_i = \vec{u}_i \vec{u}_i^T$. *Furthermore, the mass* μ^0_{jk} *of the measure* μ_{jk} *satisfies*

$$\mu^0_{jk} = \langle \chi_1 \hat{e}_k \cdot \hat{e}_k \rangle \, \delta_{jk} = d p_1^k \, \delta_{jk}. \tag{2.32}$$

Here, we have defined $p_1^k = \langle N_1^k(\omega) \rangle / N$ *to be the average number fraction of type-one bonds in the* k^{th} *direction, where* $N_1^k(\omega) = \mathrm{Trace}(\chi_1^k(\omega))$ *is the total number such bonds for* $\omega \in \Omega$, *with* $N_1(\omega) = \sum_k N_1^k(\omega)$, *and the matrix* $\chi_1^k(\omega)$ *is defined in* (2.29).

Before we prove Theorem 2.1, we first introduce an important class of composite micro-geometries. Namely, the class of geometries such that $N_1^k(\omega)$ is a non-random constant N_1^k for all $k = 1,\ldots,d$, i.e. $N_1^k(\omega) = N_1^k$ for all $\omega \in \Omega$. Consequently, $N_1(\omega) = N_1$ for all $\omega \in \Omega$ with $N_1 = \sum_k N_1^k$ and $p_1^k = N_1^k / N$ with $p_1 = \sum_k p_1^k$. Given a fixed number fraction $p_1 = N_1/N$ of type-one bonds, one can define a class of highly *anisotropic* composite geometries by fixing p_1^k close to p_1 for some $k = 1,\ldots,d$, i.e. $p_1 - p_1^k \ll 1$. A class of *locally isotropic* random media is obtained by requiring that every bond emanating from $\vec{x} \in \mathbb{Z}_L^d$ in the positive direction is of the same type, i.e. $\chi_1^j(\omega) = \chi_1^k(\omega)$ hence $N_1^j(\omega) = N_1^k(\omega)$ for all $j,k = 1,\ldots,d$ and $\omega \in \Omega$. In this case $N_1^k(\omega) = N_1/d$, thus $p_1^k = p_1/d$ for all $k = 1,\ldots,d$ and $\omega \in \Omega$. Consequently, equation (2.32) yields

$$\mu^0_{jk} = p_1 \, \delta_{jk}, \tag{2.33}$$

which is a direct analogue of equation (2.13) for the continuum setting. Equation (2.33) also holds for *statistically isotropic* random media, where each of the N bonds are chosen (independently) to be type-one with probability $p_1 = N_1/N$ and type-two with probability $1 - p_1$. In this case the $N_1^k(\omega)$, $k = 1,\ldots,d$, are independent, identically distributed random variables with mean $\langle N_1^k(\omega) \rangle = p_1 N/d$. (IS THIS PRECISELY TRUE?)

We note that, by the law of large numbers [19], the formula $\mu^0_{jk} = d p_1^k \, \delta_{jk}$ in equation (2.32) also holds in the infinite lattice setting, where $p_1^k = \lim_{N\to\infty} \langle N_1^k(\omega) \rangle / N$ is the volume fraction of type-one bonds in the k^{th} direction. Here, the infinite lattice is obtained as the infinite volume limit $L \to \infty$ ($N \to \infty$) of the finite lattice. Consequently, equation (2.33) also holds in the infinite lattice setting for locally and statistically isotropic random media. (IS THIS TRUE?)

Proof of Theorem 2.1. Taking $\vec{E} = \vec{E}_0 + \vec{E}_f$ with the condition $\Gamma \vec{E} = \vec{E}_f$ as a definition greatly simplifies the proof of Theorem 2.1, by avoiding the formulation and proof of some technical lemmas regarding the commutativity of the matrices D_j, D_j^T, and (Δ^{-1}) for $j = 1,\ldots,d$. This is a natural assumption to make, since in equation (2.15) we showed that the condition $\Gamma \vec{E} = \vec{E}_f$ is sufficient for the energy constraint $\langle \vec{J} \cdot \vec{E}_f \rangle = 0$, which is at the heart of the existence of solutions to equations (2.3) and (2.20) in the (infinite) continuum and lattice settings, respectively. In the finite lattice setting where Γ and χ_1 are matrices, this condition leads to equation (2.9) exactly as in Section (2.1), which is equivalent to the formula $(sI - \Gamma\chi_1)\vec{E} = s\vec{E}_0$ and the resolvent representation of the electric field in (2.7). As discussed above in this

section, the matrix $\Gamma\chi_1$ is not symmetric and we therefore multiply this formula by the matrix χ_1, yielding the following equation involving the real-symmetric random matrix $M_1 = \chi_1\Gamma\chi_1$

$$(s\chi_1 - \chi_1\Gamma\chi_1)\vec{E} = s\chi_1\vec{E}_0. \tag{2.34}$$

Define the sets $\mathbb{N}_L^1(\omega)$ and $\mathbb{N}_L^0(\omega)$ by

$$\mathbb{N}_L^1(\omega) = \{i \in \mathbb{N}_L \mid (\chi_1(\omega))_{ii} = 1\}, \qquad \mathbb{N}_L^0(\omega) = \mathbb{N}_L \backslash \mathbb{N}_L^1(\omega). \tag{2.35}$$

Also, define elementary permutation matrices [17] $\Pi_{i,j}$, $i,j = 1,\ldots,N$, such that $\Pi_{i,j} = \Pi_{i,j}^{-1} = \Pi_{i,j}^T$ and $\Pi_{i,j}\vec{\xi}$ is the vector $\vec{\xi}$ with the i^{th} and j^{th} entries interchanged. Since $\chi_1(\omega)$ is a diagonal matrix with $N_1(\omega)$ ones and $N_0(\omega)$ zeros along it's main diagonal, it is clear that there exists a permutation matrix $\Pi(\omega)$ such that, for each $\omega \in \Omega$,

$$\Pi(\omega)\chi_1(\omega)\Pi^T(\omega) = \begin{bmatrix} 0_{00} & 0_{01} \\ 0_{10} & I_1 \end{bmatrix}, \quad \Pi(\omega) = \prod_{i,j \in \mathbb{N}_L} \Pi_{i,j}(\omega), \tag{2.36}$$

where $i \in \mathbb{N}_L^1(\omega)$, $j \in \mathbb{N}_L^0(\omega)$, and I_1 is the identity matrix of size $N_1(\omega) \times N_1(\omega)$. Therefore, as $\Pi^T = \Pi^{-1}$ we have

$$\begin{aligned} \chi_1\Gamma\chi_1 &= \Pi^T \begin{bmatrix} 0_{00} & 0_{01} \\ 0_{10} & I_1 \end{bmatrix} \Gamma_\Pi \begin{bmatrix} 0_{00} & 0_{01} \\ 0_{10} & I_1 \end{bmatrix} \Pi = \Pi^T \begin{bmatrix} 0_{00} & 0_{01} \\ 0_{10} & \Gamma_1 \end{bmatrix} \Pi = \Pi^T \begin{bmatrix} 0_{00} & 0_{01} \\ 0_{10} & U_1\Lambda_1 U_1^T \end{bmatrix} \Pi \\ &= \Pi^T \begin{bmatrix} I_0 & 0_{01} \\ 0_{10} & U_1 \end{bmatrix} \begin{bmatrix} 0_{00} & 0_{01} \\ 0_{10} & \Lambda_1 \end{bmatrix} \begin{bmatrix} I_0 & 0_{01} \\ 0_{10} & U_1^T \end{bmatrix} \Pi, \end{aligned} \tag{2.37}$$

where $\Gamma_\Pi = \Pi\Gamma\Pi^T$, Γ_1 is the (real-symmetric) lower right principal sub-matrix of Γ_Π of size $N_1(\omega) \times N_1(\omega)$, and $\Gamma_1 = U_1\Lambda_1 U_1^T$ is its eigenvalue decomposition. As Γ_1 is a real-symmetric matrix, U_1 is an orthogonal matrix. Moreover, since $\Gamma_\Pi = \Pi\Gamma\Pi^T$ is a similarity transformation of a projection matrix and $\Pi\chi_1\Pi^T$ is a projection matrix, Λ_1 is a diagonal matrix with entries $\lambda_j^{\Pi_1} \in [0,1]$, $j = 1,\ldots,N_1(\omega)$, along the main diagonal [17]. Equation (2.37) and $\chi_1\Gamma\chi_1 = U\Lambda U^T$ imply equation (2.30) in the statement of the theorem, where U is an orthogonal matrix and Λ is a diagonal matrix with entries $\lambda_j \in [0,1]$, $j = 1,\ldots,N$, along the main diagonal.

From $\Pi^{\mathbf{T}} = \Pi^{-1}$ and equations (2.34), (2.36), and (2.37) we have

$$\begin{bmatrix} 0_{00} & 0_{01} \\ 0_{10} & (sI_1 - U_1\Lambda_1 U_1^T) \end{bmatrix} \Pi\vec{E} = \begin{bmatrix} 0_{00} & 0_{01} \\ 0_{10} & sI_1 \end{bmatrix} \Pi\vec{E}_0. \tag{2.38}$$

Define the coordinate system such that $\vec{E}_0 = E_0\hat{e}_j$, for some $j = 1,\ldots,d$, and write

$$\Pi\vec{E} = \begin{bmatrix} \vec{E}^{\Pi_0} \\ \vec{E}^{\Pi_1} \end{bmatrix}, \quad \Pi\vec{E}_0 = \begin{bmatrix} \vec{E}_0^{\Pi_0} \\ \vec{E}_0^{\Pi_1} \end{bmatrix} = E_0 \begin{bmatrix} \hat{e}_j^{\Pi_0} \\ \hat{e}_j^{\Pi_1} \end{bmatrix}, \quad \Pi\vec{u}_i = \begin{bmatrix} \vec{u}_i^{\Pi_0} \\ \vec{u}_i^{\Pi_1} \end{bmatrix}, \tag{2.39}$$

where $\vec{E}^{\Pi_0} \in \mathbb{R}^{N_0}$, $\vec{E}^{\Pi_1} \in \mathbb{R}^{N_1}$, and similarly for the vectors $\Pi\vec{E}_0$ and $\Pi\vec{u}_i$. From equation (2.38) we have $(sI_1 - U_1\Lambda_1 U_1^T)\vec{E}^{\Pi_1} = s\vec{E}_0^{\Pi_1}$, which yields the following resolvent representation for $\vec{E}^{\Pi_1}$ that is a direct analogue of equation (2.7)

$$\vec{E}^{\Pi_1} = s(sI_1 - U_1\Lambda_1 U_1^T)^{-1}\vec{E}_0^{\Pi_1}, \quad s \in \mathbb{C}\backslash[0,1]. \tag{2.40}$$

Equation (2.40) leads to a Stieltjes integral representation for $\boldsymbol{\sigma}^*$ with components $\sigma^*_{jk} = \boldsymbol{\sigma}^* \hat{e}_j \cdot \hat{e}_k$ as follows. Recall the definition of the effective complex conductivity tensor $\boldsymbol{\sigma}^*$:

$$\boldsymbol{\sigma}^* \vec{E}_0 = \langle \vec{J} \rangle = \sigma_2 \langle (1 - \chi_1/s)\vec{E} \rangle = \sigma_2 (\vec{E}_0 - \langle \chi_1 \vec{E} \rangle / s). \tag{2.41}$$

Since the symmetric matrix χ_1 satisfies $\chi_1^2 = \chi_1$ and $\Pi^T = \Pi^{-1}$, equations (2.36) and (2.39) yield the following projection identity

$$\chi_1 \vec{E} \cdot \hat{e}_k = \vec{E}^{\Pi_1} \cdot \hat{e}_k^{\Pi_1}. \tag{2.42}$$

Therefore, equations (A-4), (2.35), and (2.39)–(2.42) imply that

$$\begin{aligned} \delta_{ij} - \sigma^*_{jk}/\sigma_2 &= \langle \chi_1 \vec{E} \cdot \hat{e}_k \rangle / (sE_0) = \langle \vec{E}^{\Pi_1} \cdot \hat{e}_k^{\Pi_1} \rangle / (sE_0) \\ &= \langle (sI_1 - U_1 \Lambda_1 U_1^T)^{-1} \hat{e}_j^{\Pi_1} \cdot \hat{e}_k^{\Pi_1} \rangle = \sum_{i \in \mathbb{N}_L^1} \left\langle \frac{R_i^{\Pi_1} \hat{e}_j^{\Pi_1}}{s - \lambda_i^{\Pi_1}} \cdot \hat{e}_k^{\Pi_1} \right\rangle, \end{aligned} \tag{2.43}$$

where $R_i^{\Pi_1}$, $i \in N_L^1(\omega)$, is the projection matrix of size $N_1(\omega) \times N_1(\omega)$ associated with the columns $\vec{u}_i^{\Pi_1}$ of the orthogonal matrix U_1.

We now show that equation (2.43) is equivalent to equation (2.31). Since $\Pi^T = \Pi^{-1}$, equations (2.30) and (2.36) imply that

$$\chi_1 U = \Pi^T \begin{bmatrix} 0_{00} & 0_{01} \\ 0_{10} & U_1 \end{bmatrix}. \tag{2.44}$$

Recalling the definitions of $\vec{u}_i$ and R_i from the statement of the theorem, equation (2.44) implies that

$$\chi_1 \vec{u}_i = \begin{cases} \vec{u}_i, & \text{for } i \in \mathbb{N}_L^1 \\ 0, & \text{for } i \in \mathbb{N}_L^0 \end{cases} \quad \Rightarrow \quad \chi_1 R_i = \begin{cases} R_i, & \text{for } i \in \mathbb{N}_L^1 \\ 0, & \text{for } i \in \mathbb{N}_L^0 \end{cases}. \tag{2.45}$$

Similar to equation (2.42) we have the projection identity $\vec{u}_i^{\Pi_1} \cdot \hat{e}_j^{\Pi_1} = \chi_1 \vec{u}_i \cdot \hat{e}_j$. This and equation (2.45) yield another important projection identity

$$R_i^{\Pi_1} \hat{e}_j^{\Pi_1} \cdot \hat{e}_k^{\Pi_1} = (\vec{u}_i^{\Pi_1} \cdot \hat{e}_j^{\Pi_1})(\vec{u}_i^{\Pi_1} \cdot \hat{e}_k^{\Pi_1}) = (\chi_1 \vec{u}_i \cdot \hat{e}_j)(\chi_1 \vec{u}_i \cdot \hat{e}_k) = \chi_1 R_i \hat{e}_j \cdot \hat{e}_k.$$

Therefore, equation (2.45) implies that

$$\sum_{i \in \mathbb{N}_L^1} \left\langle \frac{R_i^{\Pi_1} \hat{e}_j^{\Pi_1}}{s - \lambda_i^{\Pi_1}} \cdot \hat{e}_k^{\Pi_1} \right\rangle = \sum_{i \in \mathbb{N}_L^1} \left\langle \frac{\chi_1 R_i \hat{e}_j}{s - \lambda_i^{\Pi_1}} \cdot \hat{e}_k \right\rangle = \sum_{i=1}^{N} \left\langle \frac{\chi_1 R_i \hat{e}_j}{s - \lambda_i} \cdot \hat{e}_k \right\rangle,$$

which proves our claim that equation (2.43) is equivalent to equation (2.31). Note that the equivalence of equations (2.43) and (2.31) implies that the spectral measure μ_{jk} in (2.31) satisfies

$$\mu_{jk}(d\lambda) = \sum_{i=1}^{N} \langle \delta_{\lambda_i}(d\lambda) \chi_1 R_i \hat{e}_j \cdot \hat{e}_k \rangle \equiv \sum_{i \in \mathbb{N}_L} \langle \delta_{\lambda_i^{\Pi_1}}(d\lambda) R_i^{\Pi_1} \hat{e}_j^{\Pi_1} \cdot \hat{e}_k^{\Pi_1} \rangle. \tag{2.46}$$

We now discuss the analogue of equation (2.13) for the finite lattice setting and prove equation (2.32) in the statement of the theorem. Recall that the projection

matrices $R_i^{\Pi_1}$, $i\in\mathbb{N}_L$, are symmetric. Therefore, by equations (A-2) and (2.46) we have

$$\mu_{jk}^0=\int_0^1\mu_{jk}(d\lambda)=\int_0^1\sum_{i=1}^N\langle\delta_{\lambda_i}(d\lambda)\chi_1R_i\hat{e}_j\cdot\hat{e}_k\rangle=\langle\chi_1\hat{e}_j\cdot\hat{e}_k\rangle=\langle\chi_1\hat{e}_k\cdot\hat{e}_k\rangle\,\delta_{jk},$$
$$\mu_{kk}(d\lambda)=\sum_{i\in\mathbb{N}_L}\langle\delta_{\lambda_i^{\Pi_1}}(d\lambda)R_i^{\Pi_1}\hat{e}_k^{\Pi_1}\cdot\hat{e}_k^{\Pi_1}\rangle=\sum_{i\in\mathbb{N}_L}\langle\delta_{\lambda_i^{\Pi_1}}(d\lambda)|R_i^{\Pi_1}\hat{e}_k^{\Pi_1}|^2\rangle, \tag{2.47}$$

where $|\cdot|$ denotes the l^2 norm on $\mathbb{R}^{N_1(\omega)}$. Therefore, as in the continuum setting, the diagonal components μ_{kk} of the matrix valued measure $\boldsymbol{\mu}$ are positive measures of mass $\langle\chi_1\hat{e}_k\cdot\hat{e}_k\rangle$ while the off-diagonal components μ_{jk}, for $j\neq k$, have zero mass and are consequently signed measures. Using equation (2.29) we may write μ_{jk}^0 in (2.47) in a more suggestive form. Recall that $\hat{e}_1=(\vec{1},\vec{0},\ldots,\vec{0})/L^{d/2}$, where $\vec{1}$ and $\vec{0}$ are vectors of ones and zeros of length L^d, respectively, and similarly for the $\vec{e}_j$ for $j=2,\ldots,d$ (see Section 2.2.2 for details). Since χ_1 is a symmetric projection matrix, equations (2.29) and (2.47) imply that

$$\mu_{jk}^0=\langle\chi_1\hat{e}_k\cdot\chi_1\hat{e}_k\rangle\,\delta_{jk}=\frac{1}{L^d}\langle\chi_1^k\vec{1}\cdot\chi_1^k\vec{1}\rangle\,\delta_{jk}=\frac{1}{L^d}\langle\mathrm{Trace}(\chi_1^k)\rangle\,\delta_{jk}=d\frac{\langle N_1^k(\omega)\rangle}{N}\delta_{jk}, \tag{2.48}$$

where $N_1^k(\omega)=\mathrm{Trace}(\chi_1^k(\omega))$ is the total number of type-one bonds in the positive k^{th} direction for $\omega\in\Omega$ and $N=dL^d$. This proves equation (2.32) and concludes our proof of Theorem 2.1 $\square$.

2.3. Bounding Procedure A key feature of the integral representation for $F_{jk}(s)$, $j,k=1,\ldots,d$, displayed in equations (2.10) and (2.31), is that parameter information in s and E_0 is *separated* from the geometry of the composite, which is encoded in the spectral measure μ_{jk} via its moments μ_{jk}^n, $n=0,1,2,\ldots$ [10, 28]. Another important feature of the representation for $F_{jk}(s)$ is that it is a *linear* functional of the measure μ_{jk}. Moreover, the diagonal components μ_{kk} are *positive* measures. These properties are also shared by the function $E_{jk}(s)$ given in equation (2.10) and its discrete counterpart in (2.31). These important properties may be exploited to obtain rigorous bounds for the diagonal components of the effective parameters [6, 7, 37, 28, 8]. In this section we review a bounding procedure which is presented in [28, 22]. The bounds incorporate the moments μ_{kk}^n and η_{kk}^n, $n=0,1,2,\ldots$, of the measures μ_{kk} and η_{kk} associated with the functions $F_{kk}(s)$ and $E_{kk}(s)$, respectively. It is therefore appropriate to start our discussion with the masses μ_{kk}^0 and η_{kk}^0 of these measures for the continuum and lattice settings.

By equation (2.13) and the symmetries between the functions $F_{kk}(s)$ and $E_{kk}(s)$ displayed in equation (2.10), in the continuum setting the masses of these measures are generically given by $\mu_{kk}^0=p_1$ and $\eta_{kk}^0=p_2$. By equation (2.32), in the finite lattice setting we have $\mu_{kk}^0=dp_1^k$. The masses μ_{kk}^0 and η_{kk}^0 of the measures μ_{kk} and η_{kk} are related in this lattice setting as follows. Note that $\chi_1^k(\omega)+\chi_2^k(\omega)=I_{L^d}$ for all $k=1,\ldots,d$ and $\omega\in\Omega$, where I_{L^d} is the identity matrix of size $L^d\times L^d$. By the linearity of the trace operation, we therefore have $\mathrm{Trace}(\chi_1^k(\omega))+\mathrm{Trace}(\chi_2^k(\omega))=\mathrm{Trace}(I_{L^d})$ or equivalently $N_1^k(\omega)+N_2^k(\omega)=L^d=N/d$. Averaging this formula over Ω and rearranging yields

$$\mu_{kk}^0+\eta_{kk}^0=1,\quad k=1,\ldots,d, \tag{2.49}$$

where $\eta^0_{kk} = dp_2^k$ and $p_2^k = \langle N_2^k(\omega)\rangle/N$ is the average number fraction of type-two bonds in the k^{th} direction. For isotropic random media we have by equation (2.33) $\mu^0_{kk} = p_1$ and $\eta^0_{kk} = p_2$. By the discussion in the paragraph following this equation the formulas $\mu^0_{kk} = dp_1^k$ and $\eta^0_{kk} = dp_2^k$ also hold for the infinite lattice setting with $p_i^k = \lim_{N\to\infty}\langle N_i(\omega)\rangle/N$, $i = 1,2$, and are given by $\mu^0_{kk} = p_1$ and $\eta^0_{kk} = p_2$ for isotropic random media.

In this section, we will discuss the bounding procedure in terms of the diagonal components σ^*_{kk}, $k = 1,\ldots,d$, of the effective complex conductivity tensor $\boldsymbol{\sigma}^*$. For simplicity, we will focus on one such component and set $\sigma^* = \sigma^*_{kk}$, $F(s) = F_{kk}(s)$, $m(h) = m_{kk}(h)$, $\mu = \mu_{kk}$, $E(s) = E_{kk}(s)$, $\tilde{m}(h) = \tilde{m}_{kk}(h)$, and $\eta = \eta_{kk}$. Here, $\sigma^* = \sigma_2 m(h) = \sigma_1/\tilde{m}(h)$, $F(s) = 1 - m(h)$, and $E(s) = 1 - \tilde{m}(h)$. We will also exploit the symmetries between $F(s)$ and $E(s)$ in equation (2.10) and initially focus on the function $F(s)$ and the measure μ, introducing the function $E(s)$ and the measure η when appropriate.

Bounds on σ^* are obtained as follows. The support of the measure μ is contained in the interval $[0,1]$ and its mass is given by $\mu^0 = p_1$, where $0 \le p_1 \le 1$. Consider the set $\mathscr{M}$ of positive Borel measures on $[0,1]$ with mass ≤ 1. By equation (2.10), for fixed $s \in \mathbb{C}\backslash[0,1]$, $F(s)$ is a linear functional of the measure μ, $F : \mathscr{M} \mapsto \mathbb{C}$, and we write $F(s) = F(s,\mu)$ and $m(h) = m(h,\mu)$. Suppose that we know the moments μ^n of the measure μ for $n = 1,\ldots,J$. Define the set $\mathscr{M}_J^\mu \subset \mathscr{M}$ by

$$\mathscr{M}_J^\mu = \left\{ \nu \in \mathscr{M} \;\middle|\; \int_0^1 \lambda^n \nu(d\lambda) = \mu^n,\ n = 0,\ldots,J \right\}. \tag{2.50}$$

The set $A_J^\mu \subset \mathbb{C}$ that represents the possible values of $m(h,\mu) = 1 - F(s,\mu)$ which is compatible with the known information about the random medium is given by

$$A_J^\mu = \{\ m(h,\mu) \in \mathbb{C} \mid\ \ h \notin (-\infty,0],\ \mu \in \mathscr{M}_J^\mu \}. \tag{2.51}$$

The set of measures $\mathscr{M}_J^\mu$ is a compact, convex subset of $\mathscr{M}$ with the topology of weak convergence [28]. Since the mapping $F(s,\mu)$ in (2.10) is linear in μ it follows that A_J^μ is a compact convex subset of the complex plane $\mathbb{C}$. The extreme points of $\mathscr{M}_0^\mu$ are the one point measures $a\delta_b$, $0 \le a,b \le 1$ [18], while the extreme points of $\mathscr{M}_J^\mu$ for $J > 0$ are weak limits of convex combinations of measures of the form [28]

$$\mu_J(d\lambda) = \sum_{i=1}^{J+1} a_i \delta_{b_i}(d\lambda), \quad a_i \ge 0, \quad 0 \le b_1 < \cdots < b_{J+1} < 1, \quad \sum_{i=1}^{J+1} a_i b_i^n = \mu^n, \tag{2.52}$$

for $n = 0,1,\ldots,J$. For the case of two-dimensional random media in the continuous setting, every measure $\mu \in \mathscr{M}_J^\mu$ gives rise to a function $m(h,\mu)$ that is the effective (relative) conductivity of a multi-rank laminate [40]. However, in general [28], not every measure $\mu \in \mathscr{M}_J^\mu$ gives rise to such a function $m(h,\mu)$. Therefore, the set A_J^μ will *contain* the exact range of values of the effective conductivity [28]. This is sufficient for the bounding procedure discussed in this section.

By the symmetries between the formulas in equation (2.10), the support of the measure η is contained in the interval $[0,1]$ and its mass is given by $\eta^0 = p_2 = 1 - p_1$, where $0 \le p_2 \le 1$. We can therefore define compact, convex sets $\mathscr{M}_J^\eta \subset \mathscr{M}$ and $A_J^\eta \subset \mathbb{C}$ which are analogous to those defined in equations (2.50) and (2.51), respectively, involving the function $\tilde{m}(h,\eta) = 1 - E(s,\eta)$. Moreover, the extreme points of $\mathscr{M}_0^\eta$ are the one point measures $c\delta_d$, $0 \le c,d \le 1$ while the extreme points of $\mathscr{M}_J^\eta$ are weak limits of convex combinations of measures of the form given in equation (2.52).

Consequently, in order to determine the extreme points of the sets A_J^μ and A_J^η it suffices to determine the range of values in $\mathbb{C}$ of the functions $m(h,\mu_J)=1-F(s,\mu_J)$ and $\tilde{m}(h,\eta_J)=1-E(s,\eta_J)$, respectively, where

$$F(s,\mu_J)=\sum_{i=1}^{J+1}\frac{a_i}{s-b_i}, \qquad E(s,\eta_J)=\sum_{i=1}^{J+1}\frac{c_i}{s-d_i}, \tag{2.53}$$

as the a_i, b_i, c_i, and d_i vary under the constraints given in equation (2.52). While $F(s,\mu_J)$ and $E(s,\eta_J)$ in (2.53) may not run over all points in A_J^μ and A_J^η as these parameters vary, they run over the extreme points of these sets, which is sufficient due to their convexity. It is important to note that, as the effective complex conductivity σ^* is given by $\sigma^*=\sigma_2 m(h,\mu)=\sigma_1/\tilde{m}(h,\eta)$, the regions A_J^μ and A_J^η have to be mapped to the common σ^*-plane to provide bounds for σ^*.

In this section we discuss two different bounds for σ^*. The first bound assumes that only the masses $\mu^0=p_1$ and $\eta^0=p_2$ of the measures μ and η are known. While the second bound also assumes that the random medium is statistically isotropic, so that the first moments of these measures are also known, and are given by [22]

$$\mu^1=\frac{p_1p_2}{d}, \qquad \eta^1=\frac{p_1p_2(d-1)}{d}. \tag{2.54}$$

Consider the first case, where $J=0$ in (2.53) and the volume fraction $p_1=1-p_2$ is fixed with $\mu^0=p_1$ and $\eta^0=p_2=1-p_1$, so that $F(s,\mu_J)=p_1/(s-\lambda)$ and $E(s,\eta_J)=p_2/(s-\tilde{\lambda})$. By the above discussion, the values of $F(s,\mu)$ and $E(s,\eta)$ lie inside the circles $C_0(\lambda)$ and $\tilde{C}_0(\tilde{\lambda})$, respectively, given by

$$C_0(\lambda)=\frac{\mu^0}{s-\lambda}, \quad -\infty\le\lambda\le\infty, \qquad \tilde{C}_0(\tilde{\lambda})=\frac{\eta^0}{s-\tilde{\lambda}}, \quad -\infty\le\tilde{\lambda}\le\infty. \tag{2.55}$$

In the σ^*-plane, the intersection of these two regions is bounded by two circular arcs corresponding to $0\le\lambda\le p_2$ and $0\le\tilde{\lambda}\le p_1$ in (2.55), and the values of σ^* lie inside this region [22]. These bounds are optimal [38, 8], and are obtained by a composite of uniformly aligned spheroids of material 1 in all sizes coated with confocal shells of material 2, and vice versa. The arcs are traced out as the aspect ratio varies. When the value of the component permittivities σ_1 and σ_2 are real and positive, the bounding region collapses to the interval $1/(p_1/\sigma_1+p_2/\sigma_2)\le\sigma^*\le p_1\sigma_1+p_2\sigma_2$, which are the Wiener bounds. The lower and upper bounds are obtained by parallel slabs of the two materials aligned perpendicular and parallel to the field $\vec{E}_0$, respectively [51].

Now consider the second case where $J=1$ in (2.53), the volume fraction $p_1=1-p_2$ is fixed, and the random medium is statistically isotropic so that the first moments μ^1 and η^1 of the measures μ and η are given, respectively, by that in equation (2.54). A convenient way of including this information is to use the transformations [8]

$$F_1(s)=\frac{1}{p_1}-\frac{1}{sF(s)}, \qquad E_1(s)=\frac{1}{p_2}-\frac{1}{sE(s)}. \tag{2.56}$$

Due to the symmetries between $F_1(s)$ and $E_1(s)$ in (2.56) we will first focus on the function $F_1(s)$ and introduce the function $E_1(s)$ when appropriate. The function $F_1(s)$ is an upper half plane function analytic off $[0,1]$ and therefore has an integral representation [8, 22] analogous to that in equation (2.10), involving a measure μ_1,

say, which is supported in the interval $[0,1]$. Since only the mass $\mu^0 = p_1$ and the first moment $\mu^1 = p_1 p_2/d$ of the measure μ are known, the transformation (2.56) determines only the mass $\mu_1^0 = p_2/(p_1 d)$ of the measure μ_1 [8, 22]. This reveals the utility of the transformation $F_1(s)$ in (2.56), it reduces the second case ($J=1$) for $F(s)$ to the first case ($J=0$) for $F_1(s)$.

By our previous analysis, the values of $F_1(s)$ lie inside a circle $p_2/(p_1 d(s-\lambda))$, $-\infty \le \lambda \le \infty$. Similarly, the values of $E_1(s)$ lie inside a circle $p_1(d-1)/(p_2 d(s-\tilde{\lambda}))$, $-\infty \le \tilde{\lambda} \le \infty$. Since F and E are fractional linear in F_1 and E_1, respectively, these circles are transformed to the circles $C_1(\lambda)$ in the F-plane and $\tilde{C}_1(\tilde{\lambda})$ in the E-plane given by [22]

$$C_1(\lambda) = \frac{p_1(s-\lambda)}{s(s-\lambda-p_2/d)}, \quad \tilde{C}_1(\tilde{\lambda}) = \frac{p_2(s-\tilde{\lambda})}{s(s-\tilde{\lambda}-p_1(d-1)/d)}, \qquad -\infty \le \lambda, \tilde{\lambda} \le \infty. \tag{2.57}$$

In the σ^*-plane the intersection of these two circular regions is bounded by two circular arcs [22] corresponding to $0 \le \lambda \le (d-1)/d$ and $0 \le \tilde{\lambda} \le 1/d$ in (2.57).

The vertices of the region, $C_1(0) = p_1/(s-p_2/d)$ and $\tilde{C}(0) = p_2/(s-p_1(d-1)/d)$, are attained by the Hashin–Shtrikman geometries (spheres of all sizes of material 1 in the volume fraction p_1 coated with spherical shells of material 2 in the volume fraction p_2 filling all of $\mathbb{R}^d$, and vice versa), and lie on the arcs of the first order bounds [22]. While there are at least five points on the arc $C_1(\lambda)$ in (2.57) that are attainable by composite microstructures [38], the arc $\tilde{C}_1(\tilde{\lambda})$ in (2.57) violates [22] the interchange inequality $m(h)m(1/h) \ge 1$ [36, 52], which becomes an equality in two dimensions [40]. Consequently the isotropic bounds in (2.57) are not optimal, but have been improved [37, 8] by incorporating the interchange inequality. When σ_1 and σ_2 are real and positive with $\sigma_1 \le \sigma_2$, the region collapses to the interval

$$\sigma_1 + p_2 \Big/ \left(\frac{1}{\sigma_2 - \sigma_1} + \frac{p_1}{d\sigma_1} \right) \le \sigma^* \le \sigma_1 + p_1 \Big/ \left(\frac{1}{\sigma_1 - \sigma_2} + \frac{p_2}{d\sigma_2} \right),$$

which are the Hashin–Shtrikman bounds.

The higher moments μ^n, $n \ge 2$ depend on $(n+1)$-point correlation functions [28] and cannot be calculated in general, although the interchange inequality forces relations among them [39]. If the moments $\mu^0, \ldots, \mu^J$ are known then the transformation F_1 in (2.56) can be iterated to produce an upper half plane function F_J with a integral representation, involving a positive measure μ_J which is supported on the interval $[0,1]$. As in the case where $J=1$, the first J moments of the measure μ determine only the mass μ_J^0 of the measure μ_J [22], and the function $F_J(s)$ can easily be extremized by the above procedure, and similarly for a function $E_J(s)$ associated with the moments $\eta^0, \ldots, \eta^J$. The resulting bounds form a nested sequence of lens-shaped regions [22].

3. Numerical Results In Section 2.2.2 we developed the ACM for representing transport in two-phase random media, for the finite lattice setting. Here, we demonstrate how this mathematical framework can be utilized to compute spectral measures and the associated effective parameters for such composite media. In particular, in this finite lattice setting, the spectral measures are given explicitly in terms of the eigenvalues and eigenvectors of matrix representations for the random operators $M_i = \chi_i \Gamma \chi_i$ and $K_i = \chi_i \Upsilon \chi_i$, as displayed in equation (2.31). Specifically, we employ the projection method summarized by equations (2.30) and (2.46) of Theorem 2.1

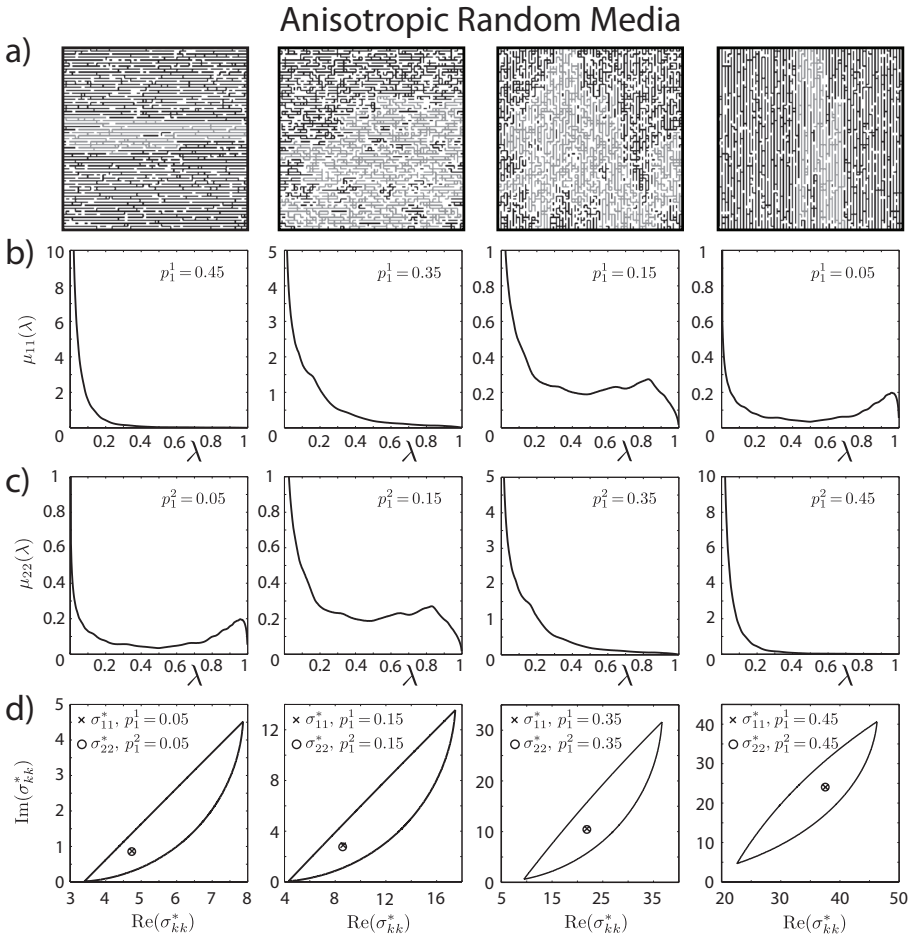

FIG. 3.1. *Spectral measures and effective complex conductivities for anisotropic random media. Statistical realizations of the 2D square bond lattice for* $p_1 = 0.5$ *and various values of* p_1^k, $k = 1,2$, *are displayed in (a), while the corresponding spectral functions* $\mu_{11}(\lambda)$ *and* $\mu_{22}(\lambda)$ *are displayed below in (b) and (c), respectively. The effective complex conductivities* σ_{11}^* *and* σ_{22}^* *are displayed in (d) for* $p_1^1 = p_1^2$, *along with the associated first-order bounds. The computed spectral functions have been rescaled so that the area under the graph is the measure mass* $\mu_{kk}^0 = dp_1^k$.

to directly calculate the spectral measures and effective parameters for the classes of locally isotropic, statistically isotropic, and anisotropic random media introduced in the paragraph after the statement of this theorem.

As the system size L increases, the size $N = dL^d$ of the matrix M_1, for example, also increases and its eigenvalues become increasingly dense in the spectral interval $[0,1]$. For a large enough fixed system, or for a random system averaged over many statistical realizations, a high resolution histogram representation of the spectral measure μ_{11}, called the *spectral function* $\mu_{11}(\lambda)$, begins to resemble a smooth curve, as shown in Figure 3.1. In Figure 3.1(a) statistical realizations of the anisotropic 2D bond lattice are displayed for $L = 60$ and a volume (number) fraction $p_1 = 0.5$ of type-one bonds, with various values of p_1^k, $k = 1,2$, the volume fraction of type-one bonds in the positive k^{th} direction. Here, the type-one bonds are colored black, while the

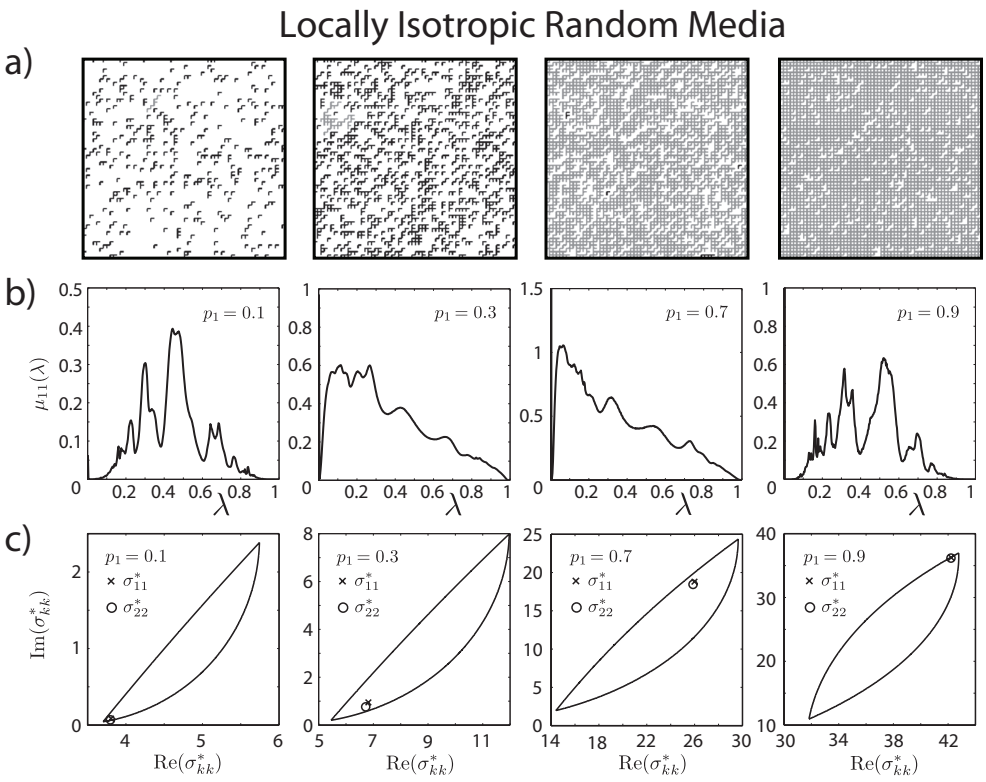

FIG. 3.2. *Spectral measures and effective complex conductivities for locally isotropic random media. Realizations of the two-dimensional lattice model are displayed in (a) with the corresponding spectral function $\mu_{11}(\lambda)$ in (b) and effective complex conductivity σ^*_{11} in (c), along with the corresponding isotropic bounds. The computed spectral functions have been rescaled so that the area under the graph is the measure mass $\mu^0_{11} = p_1$.*

largest connected cluster of type-one bonds is colored grey. In Figure 3.1(b) and (c), we display the behavior of the spectral functions $\mu_{11}(\lambda)$ and $\mu_{22}(\lambda)$, respectively, as a function of p_1^k, $k = 1,2$. In Figure 3.1(d) the computed values of the effective complex conductivities σ^*_{11} and σ^*_{22} are displayed. Consistent with the symmetries of the model, these spectral functions and effective complex conductivities satisfy $\mu_{11}(\lambda) = \mu_{22}(\lambda)$ and $\sigma^*_{11} = \sigma^*_{22}$ for $p_1^1 = p_1^2$. Also displayed in Figure 3.1(d) are the first order bounds of equation (2.55), which depend only on the mass $\mu^0_{kk} = dp_1^k$ of the measure μ_{kk} and the contrast parameter $s = 1/(1-\sigma_1/\sigma_2)$. The values of the component conductivities σ_1 and σ_2 are taken to be that of the brine and pure ice phase, respectively, for a sample of sea ice measured at a frequency of 4.75 GHz [4], $\sigma_1 = 51.0741 + \mathrm{i}45.1602$ and $\sigma_2 = 3.07 + \mathrm{i}0.0019$, yielding $s \approx -0.034 + \mathrm{i}0.032$.

We now consider the locally isotropic and statistically isotropic composite classes which were introduced in the paragraph following the statement of Theorem 2.1. In Figure 3.2 we display the behavior of the spectral function $\mu_{11}(\lambda)$ and the effective complex conductivity σ^*_{11} as a function of p_1, for locally isotropic random media with $L = 60$. In Figure 3.2(a), statistical realizations of the bond network are displayed, with the same bond color scheme as that in Figure 3.1(a). These spectral functions exhibit a rich resonance structure. These so called "geometric" resonances have been

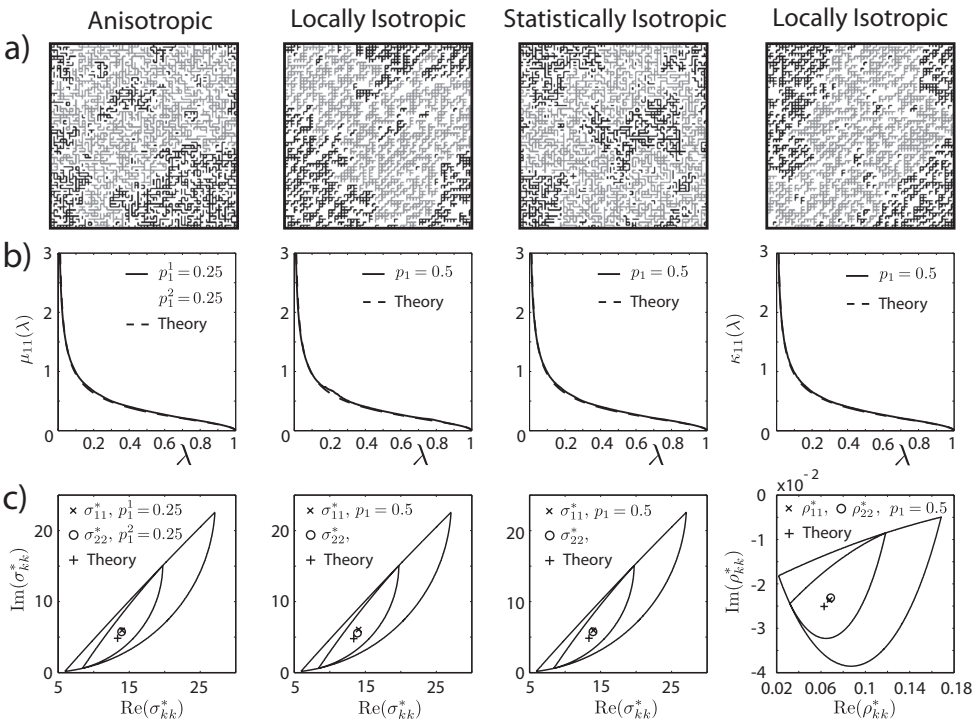

FIG. 3.3. *Statistically self-dual random media. Realizations of various two-dimensional lattice models (a) are displayed with the corresponding spectral function $\mu_{11}(\lambda)$ in (b), and effective complex conductivity σ_{11}^* or resistivity ρ_{11}^* in (c). In (b) the theoretical prediction for self-dual composite microstructures is also displayed. In (c) the effective complex conductivity or resistivity is displayed along with the theoretical prediction and the first-order and isotropic bounds. The computed spectral functions have been rescaled so that the area under the graph is the measure mass $\mu_{11}^0 = p_1$.*

attributed [34] to the recurrence of local geometric structures called "fractal animals." In Figure 3.2(c), the corresponding behavior of σ_{11}^* and σ_{22}^* is displayed along with the isotropic bounds of equation (2.57), for the same values of the component conductivities as that in Figure 3.1(c). Consistent with isotropy, the behavior of $\mu_{22}(\lambda)$ is very similar to that of $\mu_{11}(\lambda)$ in Figure 3.2(b), and to numerical accuracy and finite size effects we have $\sigma_{11}^* = \sigma_{22}^*$. The spectral functions $\mu_{kk}(\lambda)$, $k = 1,2$, in the case of statistically isotropic random media were computed in [41]. They look very similar to that for the locally isotropic case displayed in Figure 3.2(b). Moreover, the spectral functions $\kappa_{kk}(\lambda)$, $k = 1,2$, underlying the effective resistivity ρ_{kk}^*, for locally and statistically isotropic random media also look quite similar to that for $\mu_{11}(\lambda)$ in Figure 3.2(b).

In the infinite lattice setting, the statistically and locally isotropic composite microstructures for $p_1 = 0.5$ are statistically self-dual [40] (note that the anisotropic case for $p_1^1 = p_1/d$ is equivalent to the statistically isotropic case). For such systems, the spectral measures and effective parameters may be explicitly calculated [40], e.g. $\mu_{11}(d\lambda) = (\sqrt{(1-\lambda)/\lambda})(d\lambda/\pi)$ and $\sigma_{11}^* = \sqrt{\sigma_1 \sigma_2}$. In Figure 3.3 the computed spectral measures and effective parameters are displayed for such random media in the *finite* lattice setting for $L = 60$, and compared with the theoretical predictions (for the *infinite* setting). In Figure 3.3(a), the bond color scheme for the displayed statisti-

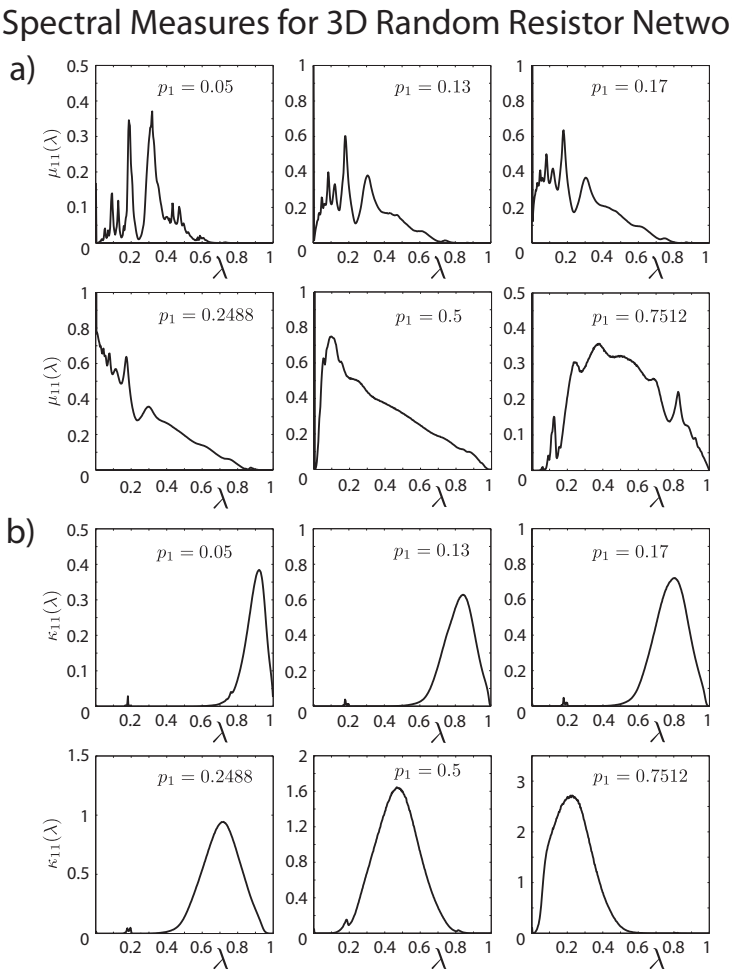

FIG. 3.4. *Spectral measures for 3D locally isotropic random resistor network. For various volume fractions p_1, the spectral function $\mu_{11}(\lambda)$ (a) underlying the effective complex conductivity σ^*_{11} is displayed with the spectral function $\kappa_{11}(\lambda)$ (b) underlying the effective complex resistivity ρ^*_{11}. The spectral functions have been rescaled so that the area under the graph is the measure mass $\mu^0_{11} = \kappa^0_{11} = p_1$.*

cal realizations is the same as that for Figure 3.1(a). In Figure 3.3(b), the computed spectral measures are displayed along with the theoretical prediction. In Figure 3.3(c) the computed effective parameters are displayed with the theoretical predictions, and the first-order and isotropic bounds of equations (2.55) and (2.57), respectively, with the same component conductivities as that in Figure 3.1(c). The computed spectral measures and effective parameters are in excellent agreement with the theoretical predictions. The error in the computed values of the effective parameters, relative to the theoretical prediction, is typically of order $\lesssim 10^{-2}$ for $L = 60$ and decreases as L increases.

We now discuss the gap behavior of the spectral measures. In the infinite lattice setting, the isotropic composite microstructures discussed in this section are examples of percolation models, which depend only on the volume fraction $p_1 = 1 - p_2$ of the

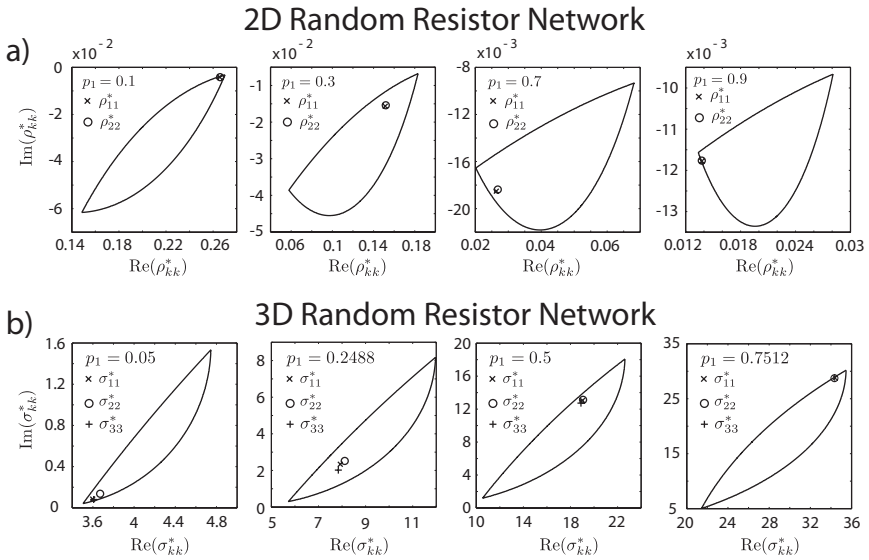

FIG. 3.5. *Effective complex parameters and isotropic bounds for 2D and 3D locally isotropic random resistor network (RRN). The behavior of the effective complex resistivity ρ^*_{kk}, $k=1,2$, for 2D RRN is displayed in (a) for various volume fractions p_1, along with the corresponding isotropic bounds. Similarly, the behavior of the effective complex conductivity σ^*_{kk}, $k=1,2,3$, and the corresponding isotropic bounds are displayed for 3D RRN in (b).*

constituents, hence $m(h)=m(p_1,h)$, for example. In these lattice percolation models [54, 56], the bonds are open with probability p_1, say, and closed with probability p_2. Connected sets of open bonds are called open clusters. The average cluster size grows as p_1 increases, and there is a critical probability p_c, $0<p_c<1$, called the *percolation threshold*, where an infinite cluster of open bonds first appears. For the two-dimensional lattice percolation model $p_c=0.5$ and $p_c\approx 0.2488$ in three-dimensions [54, 56]. Now consider transport through the associated *random resistor network* (RRN), where the bonds are assigned electrical conductivities σ_1 with probability p_1 and σ_2 with probability p_2. The effective conductivity $\sigma^*(p_1,h)$, for example, exhibits two types of critical behavior as $h=\sigma_1/\sigma_2\to 0$. First, when $\sigma_1\to 0$ and $0<\sigma_2<\infty$, $\sigma^*=0$ for $p_1>p_c$ while $\sigma^*>0$ for $p_1<p_c$. Second, when $\sigma_2\to\infty$ and $0<\sigma_1<\infty$, $\sigma^*(p_1,0)\to\infty$ as $p_1\to p_c^+$.

First we consider the two-dimensional lattice percolation model. In Figures 3.2(b) and 3.3(b) we see that, as p_1 increases from zero and the system becomes increasingly connected, gaps in the spectral function $\mu_{11}(\lambda)$ at the spectral endpoints $\lambda=0,1$ shrink and then vanish symmetrically at a value of $p_1=p_c=0.5$. Figure 3.3(b) indicates that the vanishing of the gaps in the spectral function lead to a buildup in the mass of the measure at $\lambda=0$. While the mass of the measure is approximately zero for $\lambda=1$, i.e. $\mu_{11}(1)\approx 0$.

Now consider the three-dimensional percolation model. In Figure 3.4(a) and (b) we display the behavior of the spectral functions $\mu_{11}(\lambda)$ and $\kappa_{11}(\lambda)$ as p_1 varies, for locally isotropic 3D RRN. Like its 2D counterpart, the spectral function $\mu_{11}(\lambda)$ has a rich resonant structure. Furthermore, as p_1 increases from zero and approaches the percolation threshold $p_c\approx 0.2488$, a gap in $\mu_{11}(\lambda)$ about $\lambda=0$ shrinks and then vanishes, leading to a buildup in the mass of the measure at $\lambda=0$ for $p_1=p_c$. As

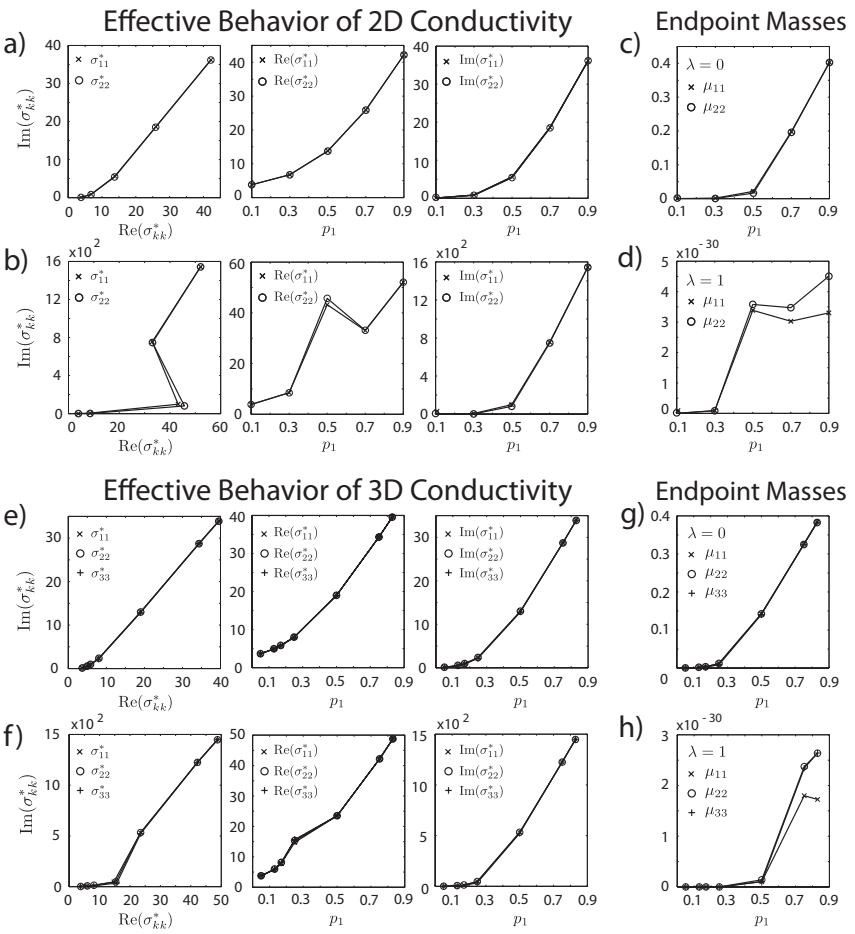

FIG. 3.6. *Behavior of the diagonal components of the effective complex conductivity tensor* $\boldsymbol{\sigma}^*$ *and the corresponding endpoint masses of the spectral measure* $\boldsymbol{\mu}$ *for 2D and 3D locally isotropic random resistor network (RRN). The behavior of the* σ^*_{kk}, $k=1,\ldots,d$, *as a function of volume fraction* p_1, *for 2D and 3D RRN is displayed for component conductivities* $\sigma_1 = 51.0741 + \mathrm{i}45.1602$ *and* $\sigma_2 = 3.07 + \mathrm{i}0.0019$ *in (a) and (e), and* $\sigma_1 = 63.3 + \mathrm{i}1930$ *and* $\sigma_2 = 3.06$ *in (b) and (f). The masses of* μ_{kk}, $k=1,\ldots,d$, *at the spectral endpoints* $\lambda = 0,1$ *corresponding to 2D RRN are given in (c) and (d), while that for 3D RRN are given in (g) and (h).*

p_1 increases beyond p_c, the eigenvalues continue to pile up at $\lambda = 0$, while a gap in the spectral function at $\lambda = 1$ shrinks and then vanishes for $p_1 = 1 - p_c \approx 0.7512$, with $\mu_{11}(1) \approx 0$. The associated behavior of the effective complex conductivity σ^*_{kk}, $k = 1,2,3$, for the 3D RRN and its corresponding bounds are displayed in Figure 3.5, as well as the effective complex resistivity ρ^*_{kk}, $k = 1,2$, for the 2D locally isotropic RRN, with the same component conductivities as that of Figure 3.1(c). The spectral measures for *statistically isotropic* 3D RRN were computed in [41] and have a very similar behavior to that for locally isotropic RRN displayed in Figure 3.4.

The behavior of the spectral function $\kappa_{11}(\lambda)$ in Figure 3.4(b) has a similar gap behavior. For a volume fraction of $p_1 = 0.001$ (not shown) there is a clear gap in the spectral function about $\lambda = 0$ and $\lambda = 1$. The gap near $\lambda = 1$ collapses as $p_1 \to p_c$, with

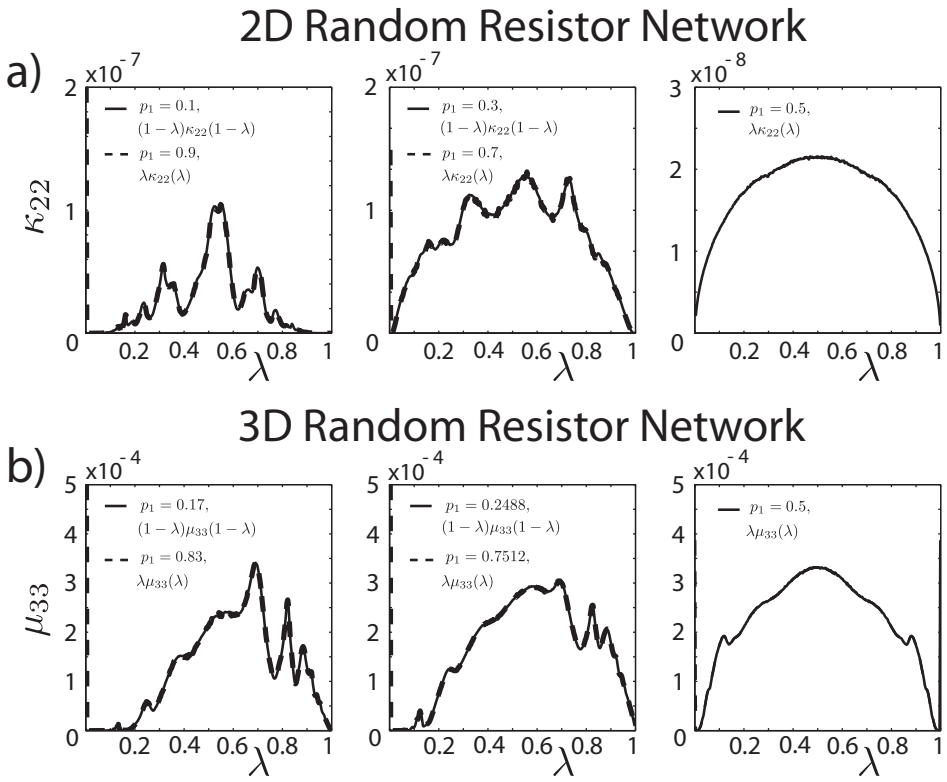

FIG. 3.7. *Spectral measure symmetries. Transformations of the computed spectral functions for 2D (a) and 3D (b) random resistor network (RRN), for various values of the volume fraction* p_1. *The computed spectral functions have* not *been rescaled to make the area under the graph the measure mass.*

$\kappa_{11}(1) \approx 0$. As p_1 surpasses p_c and approaches $1-p_c$ the gap in the spectral function near $\lambda = 0$ collapses, causing a buildup in the mass of the measure at $\lambda = 0$.

Displayed in Figure 3.6 for 2D and 3D locally isotropic RRN is the behavior of the measure mass for μ_{kk}, $k = 1,\ldots,d$, at the spectral endpoints $\lambda = 0,1$, as well as the behavior of the effective complex conductivity σ^*_{kk}, as a function of volume fraction p_1. The behavior of σ^*_{kk} displayed in Figure 3.6(a) and (e) corresponds to the same component conductivities as that in Figure 3.1(c). The behavior of σ^*_{kk} in (b) and (f) corresponds to component conductivities $\sigma_1 = 63.3 + \mathrm{i}1930$ and $\sigma_2 = 3.06$, which are that of brine and pure ice measured at a frequency of 4.75 GHz [4], yielding $s = 1/(1-\sigma_1/\sigma_2) \approx -5\times10^{-5} + \mathrm{i}0.002$. From this figure we see that the value of the contrast parameter s plays a key role in the behavior of the effective complex conductivity. Figure 3.6(c) and (g) show that, as p_1 surpasses p_c, a significant fraction of the mass of μ_{kk} is concentrated at the spectral endpoint $\lambda = 0$. This leads to significant changes in σ^*_{kk} as p_1 surpasses p_c, as can be seen in this figure. Moreover, the mass of μ_{kk} at $\lambda = 0$ is approximately zero. Please note the scale of the axes.

This behavior in the spectral measures is consistent with equation (2.12), which holds for general stationary random media in the infinite setting [41], and consequently holds for percolation models of such media. This equation characterizes the percolation transition with the formation of delta components in the spectral measures

at the spectral endpoints $\lambda=0,1$, *precisely* at $p_1=p_c$ and $p_1=1-p_c$. For example, when $\sigma_1=0$ ($h=0$) and the function $m_{kk}(0)=m_{kk}(p_1,0)$, $k=1,\ldots,d$, increases from zero as $p_1\to p_c^+$, or when $\sigma_2=0$ ($z=0$) and $w_{kk}(0)=w_{kk}(p_2,0)$ increases from zero as $p_1\to 1-p_c^-$, the masses of the delta components in the measures at $\lambda=0$ and $\lambda=1$ increase from zero, respectively, leading to critical behavior in the effective conductivity [41, 24]. Equation (2.12) also provides a relationship between the measures μ_{jk} and α_{jk}, and the measures η_{jk} and κ_{jk}. In Figure 3.7 we demonstrate that this relationship between the spectral measures holds even in the finite lattice setting.

Displayed in Figure 3.7(a) are transformations of the spectral function $\kappa_{22}(\lambda)$. In particular, the graph of the function $(1-\lambda)\kappa_{22}(1-\lambda)$ is displayed for volume fractions $p_1=0.1$, 0.3, and 0.5, along with $\lambda\kappa_{22}(\lambda)$ for a volume fraction of $1-p_1$. Similarly, in Figure 3.7(b) the graphs of $(1-\lambda)\mu_{33}(1-\lambda)$ and $\lambda\mu_{33}(\lambda)$ are displayed for various values of p_1 and $1-p_1$, respectively. The graphs of the transformed spectral functions are virtually identical except for "delta functions" at $\lambda=0,1$, in excellent agreement with equation (2.12), which holds for infinite systems.

4. Conclusion In Sections 2.1 and 2.2.1 we reviewed and extended the ACM for representing transport in composites, for the *infinite* continuum and lattice settings. This method provides the Stieltjes integral representations in (2.10) for the effective parameters of two-phase random media, involving spectral measures associated with the random operators $M_i=\chi_i\Gamma\chi_i$ and $K_i=\chi_i\Upsilon\chi_i$. Here, χ_i is the indicator function for material phase $i=1,2$ and the operators $\Gamma=\vec{\nabla}(\Delta^{-1})\vec{\nabla}\cdot$ and $\Upsilon=-\vec{\nabla}\times(\boldsymbol{\Delta}^{-1})\vec{\nabla}\times$ act as projectors onto curl-free and divergence-free fields, respectively.

In Section 2.2.2 we developed the ACM for the *finite* lattice setting. We also provided a projection method for numerically efficient, rigorous computation of spectral measures and effective parameters for such composite media. This projection method is summarized by equations (2.30) and (2.46) of Theorem 2.1, which is a key theoretical contribution of this work. In this finite lattice case, the operators χ_i, Γ, and Υ are represented by real-symmetric projection matrices, and the spectral measures of the associated matrices M_i and K_i are given explicitly in terms of their eigenvalues and eigenvectors, as displayed in equation (2.31) of Theorem 2.1.

In the paragraph following the statement of Theorem 2.1, we introduced three classes of locally isotropic, statistically isotropic, and anisotropic random media on finite bond lattices. In Section 3 we employed this projection method to compute the spectral measures and effective parameters for such composite media. To our knowledge, this is the first time that the spectral measures η_{jk} and κ_{jk} underlying the effective complex resistivity ρ^*_{jk} have been computed for such composite microstructures. These computations not only demonstrate several important properties of the spectral measures and the associated effective parameters, but they also serve as a consistency check to the theory developed here.

Consistent with general theory [40], to numerical accuracy, our computations of the effective parameters for isotropic random media satisfy $\sigma^*_{kk}=1/\rho^*_{kk}$, $k=1,\ldots,d$. Figure 3.3 demonstrates that the projection method accurately calculates the spectral measures and effective parameters for statistically self-dual composite microstructures. Furthermore, Figure 3.7 shows that the computed spectral measures are in excellent agreement with equation (2.12), which holds for general stationary two-phase random media [41].

The self-consistent mathematical framework developed here helps lay the groundwork for studies in the effective transport properties of a broad range of composite microstructures, such as electrorheological fluids [42], multiscale sea ice structures

[43], and bone [27]. Remarkably, the ACM has also been adapted to provide Stieltjes integral representations for effective parameters underlying a wide variety of transport processes, such as: the effective diffusivity for steady [2, 44] and time-dependent [3], turbulent flows, the effective complex permittivity for two-phase polycrystalline media [5, 30], and the effective elastic moduli of two-phase elastic composites [46, 47]. The Golden-Papanicolaou formulation of the ACM has been pivotal in the development of these mathematical frameworks, and in the understanding of these important transport processes.

A-1. Appendix

In this appendix we review the spectral theorem, both for the bounded linear self-adjoint operator case and the real-symmetric matrix case. This discussion provides some of the omitted mathematical details behind equations (2.10) and (2.31). We also provide a review of the Stieltjes–Perron inversion theorem and discuss how it leads to equation (2.12).

A-1.1. The Spectral Theorem Under the ACM In this section we discuss the spectral theorem [49, 55] as it pertains to the ACM. In Section A-1.1.1 we review the spectral theorem associated with the bounded linear self-adjoint operators $M_i = \chi_i \Gamma \chi_i$ and $K_i = \chi_i \Upsilon \chi_i$, $i = 1,2$, which arise naturally in the ACM for the continuum and infinite lattice settings discussed in Sections 2.1 and 2.2.1, respectively. In Section A-1.1.2 we discuss the spectral theorem for the finite lattice setting, where the operators M_i and K_i are represented by real-symmetric random matrices. In each case we obtain Stieltjes integral representations for $\boldsymbol{\sigma}^*$ and $\boldsymbol{\rho}^*$, as displayed in equations (2.10) and (2.31), involving matrix valued spectral measures.

A-1.1.1. Continuum and Infinite Lattice Settings In Section (2.1) we introduced Herglotz functions $m_{jk}(h)$, $w_{jk}(z)$, $\tilde{m}_{jk}(h)$, and $\tilde{w}_{jk}(z)$, and the respective measures μ_{jk}, α_{jk}, η_{ij}, and κ_{jk} underlying their Stieltjes integral representations. Due to the many symmetries between these functions and measures, we focused on $m_{jk}(h)$ and μ_{jk}, as the discussions involving the other functions and measures follow by direct analogy. For simplicity, we will continue this approach here.

In the paragraph proceeding that which involves equation (2.10), we argued that on the Hilbert space $\mathscr{H}_\times$ with weight χ_1 in the inner-product, $\langle \cdot, \cdot \rangle_1 = \langle \chi_1 \cdot, \cdot \rangle$, $\Gamma \chi_1$ is a bounded linear self-adjoint operator with spectrum contained in the interval $[0,1]$. By the spectral theorem for such operators, there exists an increasing family of self-adjoint projection operators $\{R(\lambda)\}$ - the resolution of the identity - that satisfy $R(0) = 0$ and $R(1) = I$ such that

$$f(M_1) = \int f(\lambda) R(d\lambda), \quad \langle f(M_1)\vec{e}_j \cdot \vec{e}_k \rangle_1 = \int_0^1 f(\lambda) \mu_{jk}(d\lambda), \tag{A-1}$$

for all bounded continuous functions $f : \mathbb{C} \mapsto \mathbb{C}$. Here 0 and I are the null and identity operators on $\mathbb{R}^d$, respectively, $R(d\lambda)$ is the projection valued measure associated with the operator $R(\lambda)$ [49], and $\mu_{jk}(d\lambda) = \langle R(d\lambda)\vec{e}_j \cdot \vec{e}_k \rangle_1$, $j,k = 1,\ldots,d$, are the components of the matrix valued *spectral measure* $\boldsymbol{\mu}(d\lambda)$ in the $(\vec{e}_j, \vec{e}_k)$ state [28, 49, 55]. As the spectrum of the operator M_1 is contained in the interval $[0,1]$, the support Σ_{jk} of the measure μ_{jk} satisfies $\Sigma_{jk} \subseteq [0,1]$ [49]. Note that setting $f(M_1) = I$ ($f(\lambda) = 1$) in equation (A-1) implies that the projection valued measure satisfies $\int_0^1 R(d\lambda) = I$. Setting $f(\lambda) = (s - \lambda)^{-1}$ in (A-1) yields the the integral formula for $F_{jk}(s)$ and $\sigma^*_{jk} = \sigma_2 m_{jk}(h)$ in equation (2.10).

A-1.1.2. Finite Lattice Setting In this section we derive a discrete version of the integral representation given in equation (A-1). This leads to the discrete integral representation for the effective conductivity tensor $\boldsymbol{\sigma}^*$ displayed in equation (2.31). Toward this goal, we defined in Section 2.2.2 a bijective mapping $\Theta : \mathbb{Z}_L^d \to \mathbb{N}_L$ from the finite d-dimensional bond lattice $\mathbb{Z}_L^d$ defined in (2.22) onto the one dimensional set $\mathbb{N}_L$ defined in equation (2.23). Moreover we showed that, under the mapping Θ, the random operator $M_1 = \chi_1 \Gamma \chi_1$ can be represented as a *real-symmetric* random matrix of size $N \times N$, where $N = dL^d$ [27, 41]. More specifically, Γ is a *non-random* real-symmetric projection matrix ($\Gamma^2 = \Gamma$) and χ_1 is a *random* diagonal projection matrix with zeros and ones along the main diagonal, and has the block diagonal form displayed in equation (2.29). Since $M_1(\omega)$ is a composition of projection matrices, it is positive definite, $M_1(\omega)\vec{\xi} \cdot \vec{\xi} = (\Gamma\chi_1(\omega)\vec{\xi}) \cdot (\Gamma\chi_1(\omega)\vec{\xi}) \geq 0$ for every $\omega \in \Omega$ and $\vec{\xi} \in \mathbb{R}^N$, and consequently has spectra $\Sigma^\lambda(\omega) \subseteq [0,1]$ [31].

It is well known [31, 35] that the eigenvectors $\vec{u}_i(\omega)$, $i = 1, \ldots, N$, of the symmetric matrix $M_1(\omega)$ form an orthonormal basis for $\mathbb{R}^N$, for each $\omega \in \Omega$, i.e., $\vec{u}_j^T \vec{u}_k = \delta_{jk}$ and for every $\vec{\xi} \in \mathbb{R}^N$ we have $\vec{\xi} = \sum_{i=1}^N (\vec{u}_i^T \vec{\xi})\vec{u}_i = \left(\sum_{i=1}^N \vec{u}_i \vec{u}_i^T\right)\vec{\xi}$. Consequently,

$$\sum_{i=1}^N R_i(\omega) = I, \quad R_i(\omega) = \vec{u}_i(\omega)\vec{u}_i^T(\omega), \quad \forall\ \omega \in \Omega, \tag{A-2}$$

where I is the identity operator on $\mathbb{R}^N$ and the matrix R_i is the orthogonal projector ($R_i R_j = R_i \delta_{ij}$) onto the eigenspace spanned by $\vec{u}_i$, which is associated with the *real* eigenvalue $\lambda_i(\omega) \in \Sigma^\lambda(\omega)$.

Since $M_1 \vec{u}_i = \lambda_i \vec{u}_i$, for each $i = 1, \ldots, N$, equation (A-2) implies that we also have $M_1 R_i = \lambda_i R_i$ which, in turn, implies that the matrix M_1 has the spectral decomposition $M_1 = \sum_{i=1}^N \lambda_i R_i$. By the orthogonality of the projection matrices R_i and by induction we have $M_1^n = \sum_{i=1}^N \lambda_i^n R_i$ for all $n \in \mathbb{N}$, which implies that $f(M_1) = \sum_{i=1}^N f(\lambda_i) R_i$ for any polynomial $f : \mathbb{C} \mapsto \mathbb{C}$. This formula is a discrete version of the first formula in equation (A-1) for polynomial $f(\lambda)$, and leads to a discrete version of the functional representation of $f(M_1)$ in (A-1) involving a matrix valued spectral measure $\boldsymbol{\mu}(d\lambda)$ with components $\mu_{jk}(d\lambda)$

$$\langle f(M_1)\hat{e}_j \cdot \hat{e}_k \rangle = \int_0^1 f(\lambda)\mu_{jk}(d\lambda), \quad \mu_{jk}(d\lambda) = \sum_{i=1}^N \langle \delta_{\lambda_i}(d\lambda) R_i \hat{e}_j \cdot \hat{e}_k \rangle. \tag{A-3}$$

Here, $R(d\lambda) = \sum_i \delta_{\lambda_i}(d\lambda) R_i$ is a discrete version of the projection valued measure introduced in equation (A-1), $\delta_{\lambda_i}(d\lambda)$ is the Dirac measure concentrated at λ_i, the orthonormal vectors $\hat{e}_i = \Theta(\vec{e}_i)/L^{d/2}$, for $i = 1, \ldots, d$, represent the standard basis vectors on $\mathbb{N}_L$, and $\langle \cdot \rangle$ denotes ensemble average over Ω. The spectral end points λ_{jk}^0 and λ_{jk}^1 of the support $\Sigma_{jk} \subseteq [\lambda_{jk}^0, \lambda_{jk}^1] \subseteq [0,1]$ of the measure μ_{jk} in (A-3) are given by $\lambda_{jk}^0 = \inf A_{jk}$ and $\lambda_{jk}^1 = \sup A_{jk}$, where

$$A_{jk} = \cup_{\omega \in \Omega} \{ \lambda_i(\omega) \in \Sigma^\lambda(\omega),\ i = 1, \ldots, N \mid R_i(\omega)\hat{e}_j \cdot \hat{e}_k \neq 0 \}$$

and $\Sigma_1^\lambda(\omega) \subseteq [0,1]$ is the support of the eigenvalues of the matrix $M_1(\omega)$ for $\omega \in \Omega$.

We now show that equation (A-3) also holds for the function $f(\lambda) = (s - \lambda)^{-1}$ when $s \notin [0,1]$. For each $\omega \in \Omega$, let $U(\omega)$ denote the matrix with columns consisting of the eigenvectors $\vec{u}_i(\omega)$ of $M_1(\omega)$ and let $\Lambda(\omega) = \mathrm{diag}(\lambda_1(\omega), \ldots, \lambda_N(\omega))$ denote the diagonal

matrix of the corresponding eigenvalues $\lambda_i(\omega)$, $i=1,\ldots,N$, so that $M_1 = U\Lambda U^T$ [31]. By the orthogonality, $U^TU = UU^T = I$, of the matrix U we have

$$\begin{aligned}\langle f(M_1)\hat{e}_j\cdot\hat{e}_k\rangle &= \langle (sI-U\Lambda U^T)^{-1}\hat{e}_j\cdot\hat{e}_k\rangle = \langle U(sI-\Lambda)^{-1}U^T\hat{e}_j\cdot\hat{e}_k\rangle \\ &= \langle (sI-\Lambda)^{-1}U^T\hat{e}_j\cdot U^T\hat{e}_k\rangle = \sum_{i=1}^{N}\left\langle \frac{R_i\hat{e}_j}{s-\lambda_i}\cdot\hat{e}_k\right\rangle.\end{aligned} \tag{A-4}$$

Equation (A-4) is equivalent to equation (A-3) when the function $f(\lambda) = (s-\lambda)^{-1}$, $s\in\mathbb{C}\backslash[0,1]$.

Acknowledgement. We gratefully acknowledge support from the Division of Mathematical Sciences at the U.S. National Science Foundation (NSF) through Grant Number DMS-1009704.

REFERENCES

[1] N. Akhiezer, *The Classical Moment Problem*, Oliver & Boyd, 1965.
[2] M. Avellaneda and A. Majda, *An integral representation and bounds on the effective diffusivity in passive advection by laminar and turbulent flows*, Comm. Math. Phys., 138 (1991), pp. 339–391.
[3] M. Avellaneda and M. Vergassola, *Stieltjes integral representation of effective diffusivities in time-dependent flows*, Phys. Rev. E, 52 (1995), pp. 3249–3251.
[4] L. Backstrom, *Capacitance Measurements of Bulk Salinity and Brine Movement in First-year Sea Ice*, University of Alaska Fairbanks, 2007.
[5] S. Barabash and D. Stroud, *Spectral representation for the effective macroscopic response of a polycrystal: application to third-order non-linear susceptibility*, J. Phys., Condens. Matter, 11 (1999), pp. 10323–10334.
[6] D. J. Bergman, *The dielectric constant of a composite material – A problem in classical physics*, Phys. Rep. C, 43 (1978), pp. 377–407.
[7] ———, *Exactly solvable microscopic geometries and rigorous bounds for the complex dielectric constant of a two-component composite material*, Phys. Rev. Lett., 44 (1980), pp. 1285–1287.
[8] ———, *Rigorous bounds for the complex dielectric constant of a two–component composite*, Ann. Phys., 138 (1982), pp. 78–114.
[9] C. Bonifasi-Lista and E. Cherkaev, *Electrical impedance spectroscopy as a potential tool for recovering bone porosity*, Phys. Med. Biol., 54 (2009), pp. 3063–3082.
[10] O. Bruno and K. Golden, *Interchangeability and bounds on the effective conductivity of the square lattice*, J. Stat. Phys., 61 (1990), p. 365.
[11] E. Cherkaev, *Inverse homogenization for evaluation of effective properties of a mixture*, Inverse Problems, 17 (2001), pp. 1203–1218.
[12] E. Cherkaev and C. Bonifasi-Lista, *Characterization of structure and properties of bone by spectral measure method*, J. Biomech., 44 (2011), pp. 345 – 351.
[13] E. Cherkaev and K. M. Golden, *Inverse bounds for microstructural parameters of composite media derived from complex permittivity measurements*, Waves in Random Media, 8 (1998), pp. 437–450.
[14] E. Cherkaev and M.-J. Ou, *De-homogenization: Reconstruction of moments of the spectral measure of composite*, Inverse Problems, 24 (2008), p. 065008 (19pp).
[15] A. R. Day and M. F. Thorpe, *The spectral function of composites: the inverse problem*, J. Phys.: Cond. Matt., 11 (1999), pp. 2551–2568.
[16] P. Deift, *Orthogonal Polynomials and Random Matrices: a Riemann–Hilbert Approach*, Courant Institute of Mathematical Sciences, New York, NY, 2000.
[17] J. W. Demmel, *Applied Numerical Linear Algebra*, SIAM, 1997.
[18] N. Dunford and J. T. Schwartz, *Linear Operators, Part I*, John Wiley & Sons, Inc., Hoboken, NJ, 1988.
[19] R. Durrett, *Probability: Theory and Examples*, 4th Edition, Cambridge U Press, 2010.
[20] G. B. Folland, *Introduction to Partial Differential Equations*, Princeton University Press, Princeton, NJ, 1995.

[21] ———, *Real Analysis: Modern Techniques and Their Applications*, Wiley–Interscience, New York, NY, 1999.
[22] K. Golden, *Bounds on the complex permittivity of a multicomponent material*, J. Mech. Phys. Solids, 34 (1986), pp. 333–358.
[23] K. M. Golden, *Exponent inequalities for the bulk conductivity of a hierarchical model*, Commun. Math. Phys., 143 (1992), pp. 467–499.
[24] ———, *Statistical mechanics of conducting phase transitions*, J. Math. Phys., 36 (1995), pp. 5627–5642.
[25] ———, *Critical behavior of transport in lattice and continuum percolation models*, Phys. Rev. Lett., 78 (1997), pp. 3935–3938.
[26] ———, *The interaction of microwaves with sea ice*, in Wave Propagation in Complex Media, IMA Volumes in Mathematics and its Applications, Vol. 96, G. Papanicolaou, ed., Springer – Verlag, 1997, pp. 75 – 94.
[27] K. M. Golden, N. B. Murphy, and E. Cherkaev, *Spectral analysis and connectivity of porous microstructures in bone*, J. Biomech., 44 (2011), pp. 337–344.
[28] K. M. Golden and G. Papanicolaou, *Bounds for effective parameters of heterogeneous media by analytic continuation*, Commun. Math. Phys., 90 (1983), pp. 473–491.
[29] ———, *Bounds for effective parameters of multicomponent media by analytic continuation*, J. Stat. Phys., 40 (1985), pp. 655–667.
[30] A. Gully, J. Lin, E. Cherkaev, and K. M. Golden, *Polycrystalline bounds on the complex permittivity of sea ice.* preprint, 2012.
[31] P. R. Halmos, *Finite Dimensional Vector Spaces*, Van Nostrand–Reinhold, Princeton, NJ, 1958.
[32] P. Henrici, *Applied and Computational Complex Analysis. Volume 2.*, John Wiley & Sons Inc., New York, 1974.
[33] J. D. Jackson, *Classical Electrodynamics*, John Wiley and Sons, Inc., New York, 1999.
[34] T. Jonckheere and J. M. Luck, *Dielectric resonances of binary random networks*, J. Phys. A: Math. Gen., 31 (1998), pp. 3687–3717.
[35] J. P. Keener, *Principles of applied mathematics: transformation and approximation*, Westview Press, Cambridge, MA, 2000.
[36] J. B. Keller, *A theorem on the conductivity of a composite medium*, J. Math. Phys., 5 (1964), pp. 548–549.
[37] G. W. Milton, *Bounds on the complex dielectric constant of a composite material*, Appl. Phys. Lett., 37 (1980), pp. 300–302.
[38] ———, *Bounds on the complex permittivity of a two component composite material*, J. Appl. Phys., 52 (1981), pp. 5286–5293.
[39] ———, *Bounds on the transport and optical properties of a two-component composite material*, J. Appl. Phys., 52 (1981), pp. 5294–5304.
[40] ———, *Theory of Composites*, Cambridge University Press, Cambridge, 2002.
[41] N. B. Murphy and K. M. Golden, *The Ising model and critical behavior of transport in binary composite media*, J. Math. Phys., 53 (2012), p. 063506.
[42] N. B. Murphy, K. M. Golden, and P. Sheng, *Statistical mechanics of homogenization for composite media.* Preprint, 20 pages (in revision before submission)., 2013.
[43] N. B. Murphy, C. Hohenegger, C. S. Sampson, D. K. Perovich, H. Eicken, E. Cherkaev, B. Alali, and K. M. Golden, *Spectral analysis of multiscale sea ice structures in the climate system.* In preparation., 2012.
[44] N. B. Murphy, J. Zhu, and K. M. Golden, *Spectral analysis of advective diffusion.* Preprint, 17 pages (in revision before submission)., 2013.
[45] C. Orum, E. Cherkaev, and K. M. Golden, *Recovery of inclusion separations in strongly heterogeneous composites from effective property measurements*, Proc. Roy. Soc. London A, 468 (2012), pp. 784–809.
[46] M. Ou, *Two-parameter integral representation formula for the effective elastic moduli of two-phase composites.*, Complex Var. Elliptic Equ., 57 (2012), pp. 411–424.
[47] M. J. Ou and E. Cherkaev, *On the integral representation formula for a two-component elastic composite*, Mathematical Methods in the Applied Sciences, 29 (2006), pp. 655–644.
[48] G. Papanicolaou and S. Varadhan, *Boundary value problems with rapidly oscillating coefficients*, in Colloquia Mathematica Societatis János Bolyai 27, Random Fields (Esztergom, Hungary 1979), North-Holland, 1982, pp. 835–873.
[49] M. C. Reed and B. Simon, *Functional Analysis*, Academic Press, San Diego CA, 1980.
[50] W. Rudin, *Real and Complex Analysis*, McGraw-Hill, Inc., New York, NY, 1987.
[51] B. K. P. Scaife, *Principles of Dielectrics*, Clarendon Press, Oxford, 1989.
[52] K. Schulgasser, *On the conductivity of fiber reinforced materials*, J. Math. Phys., 17 (1976),

pp. 382–387.

[53] L. B. Simeonova, D. C. Dobson, O. Eso, and K. M. Golden, *Spatial bounds on the effective complex permittivity for time-harmonic waves in random media*, Multiscale Modeling and Simulation, 9 (2011), pp. 1113–1143.

[54] D. Stauffer and A. Aharony, *Introduction to Percolation Theory*, Taylor and Francis, London, second ed., 1992.

[55] M. H. Stone, *Linear Transformations in Hilbert Space*, American Mathematical Society, Providence, RI, 1964.

[56] S. Torquato, *Random Heterogeneous Materials: Microstructure and Macroscopic Properties*, Springer-Verlag, New York, 2002.

[57] D. Zhang and E. Cherkaev, *Reconstruction of spectral function from effective permittivity of a composite material using rational function approximations*, J. Comput. Phys., 228 (2009), pp. 5390 – 5409.